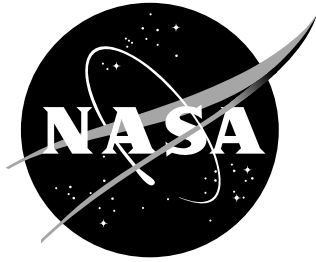


NASA/CR-1999-209544



# Investigation of a Technique for Measuring Dynamic Ground Effect in a Subsonic Wind Tunnel

*Sharon S. Graves  
The George Washington University  
Joint Institute for Advancement of Flight Sciences  
Langley Research Center, Hampton, Virginia*

---

August 1999

## The NASA STI Program Office ... in Profile

Since its founding, NASA has been dedicated to the advancement of aeronautics and space science. The NASA Scientific and Technical Information (STI) Program Office plays a key part in helping NASA maintain this important role.

The NASA STI Program Office is operated by Langley Research Center, the lead center for NASA's scientific and technical information. The NASA STI Program Office provides access to the NASA STI Database, the largest collection of aeronautical and space science STI in the world. The Program Office is also NASA's institutional mechanism for disseminating the results of its research and development activities. These results are published by NASA in the NASA STI Report Series, which includes the following report types:

- **TECHNICAL PUBLICATION.** Reports of completed research or a major significant phase of research that present the results of NASA programs and include extensive data or theoretical analysis. Includes compilations of significant scientific and technical data and information deemed to be of continuing reference value. NASA counterpart and peer-reviewed formal professional papers, but having less stringent limitations on manuscript length and extent of graphic presentations.
- **TECHNICAL MEMORANDUM.** Scientific and technical findings that are preliminary or of specialized interest, e.g., quick release reports, working papers, and bibliographies that contain minimal annotation. Does not contain extensive analysis.
- **CONTRACTOR REPORT.** Scientific and technical findings by NASA-sponsored contractors and grantees.

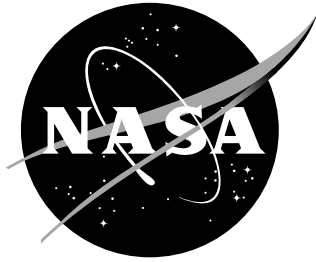
- **CONFERENCE PUBLICATION.** Collected papers from scientific and technical conferences, symposia, seminars, or other meetings sponsored or co-sponsored by NASA.
- **SPECIAL PUBLICATION.** Scientific, technical, or historical information from NASA programs, projects, and missions, often concerned with subjects having substantial public interest.
- **TECHNICAL TRANSLATION.** English-language translations of foreign scientific and technical material pertinent to NASA's mission.

Specialized services that complement the STI Program Office's diverse offerings include creating custom thesauri, building customized databases, organizing and publishing research results ... even providing videos.

For more information about the NASA STI Program Office, see the following:

- Access the NASA STI Program Home Page at <http://www.sti.nasa.gov>
- E-mail your question via the Internet to [help@sti.nasa.gov](mailto:help@sti.nasa.gov)
- Fax your question to the NASA STI Help Desk at (301) 621-0134
- Phone the NASA STI Help Desk at (301) 621-0390
- Write to:  
NASA STI Help Desk  
NASA Center for AeroSpace Information  
7121 Standard Drive  
Hanover, MD 21076-1320

NASA/CR-1999-209544



# Investigation of a Technique for Measuring Dynamic Ground Effect in a Subsonic Wind Tunnel

*Sharon S. Graves  
The George Washington University  
Joint Institute for Advancement of Flight Sciences  
Langley Research Center, Hampton, Virginia*

National Aeronautics and  
Space Administration

Langley Research Center  
Hampton, Virginia 23681-2199

Prepared for Langley Research Center  
under Cooperative Agreement NCC1-24

---

August 1999

---

Available from:

NASA Center for AeroSpace Information (CASI)  
7121 Standard Drive  
Hanover, MD 21076-1320  
(301) 621-0390

National Technical Information Service (NTIS)  
5285 Port Royal Road  
Springfield, VA 22161-2171  
(703) 605-6000

## Abstract

*To better understand the ground effect encountered by slender wing supersonic transport aircraft, a test was conducted at NASA Langley Research Center's 14 x 22 foot Subsonic Wind Tunnel in October, 1997. Emphasis was placed on improving the accuracy of the ground effect data by using a "dynamic" technique in which the model's vertical motion was varied automatically during wind-on testing. This report describes and evaluates different aspects of the dynamic method utilized for obtaining ground effect data in this test. The method for acquiring and processing time data from a dynamic ground effect wind tunnel test is outlined with details of the overall data acquisition system and software used for the data analysis. The removal of inertial loads due to sting motion and the support dynamics in the balance force and moment data measurements of the aerodynamic forces on the model is described. An evaluation of the results identifies problem areas providing recommendations for future experiments. Test results are validated by comparing test data for an elliptical wing planform with an Elliptical wing planform section with a NACA 0012 airfoil to results found in current literature. Major aerodynamic forces acting on the model in terms of lift curves for determining ground effect are presented. Comparisons of flight and wind tunnel data for the TU-144 are presented.*

## Nomenclature

Symbol	Definition
A1-6	Accelerometer measurements
AF	Axial Force, lbs
AR	Wing model aspect ratio, $b^2/S$
b	Wing model span, in
$c_o$	Wing model root chord, in
$\bar{c}$	Wing model mean geometric chord, in
c.g.	Center of gravity
$C_L$	Coefficient of lift in ground effect
$C_{L,oge}$	Coefficient of lift out of ground effect
$\%C_L$	Percent increase in lift coefficient, $[(C_L - C_{L,oge})/C_{L,oge}] \times 100$
$C_M$	Coefficient of pitching moment about the quarter-chord point of the mean aerodynamic chord in ground effect
F	Aerodynamic force, lbs
g	Gravity
h	Height of model over ground board,
$\dot{h}$	Sink rate, ft/s
$I_x$	Moment of inertia about the x-axis
$I_y$	Moment of inertia about the y-axis
$I_z$	Moment of inertia about the z-axis
m	Mass
NF	Normal Force, lbs
OGE	Out of ground effect
p	Roll angular velocity
PM	Pitching Moment, ft-lbs
q	Pitch angular velocity
Q	dynamic pressure, psf
r	Yaw angular velocity
RM	Rolling Moment, ft-lbs
S	Wing model area, $in^2$
SF	Side Force, lbs
t	Time
u	Axial velocity
v	Side velocity
w	Normal velocity
$\dot{p}$	Roll angular acceleration, $rad/s^2$
$\dot{q}$	Pitch angular acceleration, $rad/s^2$
$\dot{r}$	Yaw angular acceleration. $rad/s^2$
$\dot{u}$	Axial acceleration, $ft/s^2$
$\dot{v}$	Side acceleration, $ft/s^2$
$\dot{w}$	Normal acceleration, $ft/s^2$
YM	Yawing moment, ft-lbs

$\alpha$	Angle of attack, deg
$\Lambda_{LE}$	Leading edge sweep angle
$\theta$	Pitch angle, deg
$\phi$	Roll angle, deg
Flight path angle (incidence of model path relative to the ground plane, deg	
$\delta$	deflection angle, deg

<b>Acronym</b>	<b>Definition</b>
DGE	Dynamic Ground Effect
HSCT	High Speed Civil Transport
HSR	High Speed Research
MIF	Model Interface Rack
MPA	Model Preparation Area
OGE	Out of ground effect
TCA	Technical Configuration Aircraft

# TABLE OF CONTENTS

<b>NOMENCLATURE</b>	<b>2</b>
<b>TABLE OF CONTENTS</b>	<b>4</b>
<b>TABLE OF FIGURES</b>	<b>6</b>
<b>INTRODUCTION</b>	<b>7</b>
<b>EXPERIMENTAL APPROACH</b>	<b>9</b>
<b>PLANFORM</b>	<b>10</b>
<b>TABLE 1. PHYSICAL PROPERTIES OF THREE BASIC PLANFORMS.</b>	<b>10</b>
<b>Instrumentation</b>	<b>13</b>
<b>Measurement Technique</b>	<b>14</b>
Force and Moment Data Translation	14
Equations for Removal of Inertial Loads	15
Linear Accelerations	18
Angular Accelerations	18
Velocity Calculations	19
Sink Rate Calculation	19
Total Velocity Calculation	19
Calculated ground height, h/b	19
Flight Path Angle	20
Angle of Attack	20
Corrected Dynamic Pressure	20
Corrected Force/Moment Coefficients	20
Performance Coefficients	21
<b>RESULTS AND DISCUSSION</b>	<b>22</b>
<b>APPENDIX A INERTIAL LOADS REMOVAL</b>	<b>33</b>
<b>APPENDIX B POST-PROCESSING DATA USING COMBOA</b>	<b>52</b>
<b>B.1 Logon Procedure</b>	<b>52</b>
<b>B.2 Setting up the Comboa Processing Directory</b>	<b>52</b>

<b>B.3</b>	<b>Defining the inxxx file</b>	<b>52</b>
<b>B.3.1</b>	<b>rptname file</b>	<b>52</b>
<b>B.4</b>	<b>Comboa user interface</b>	<b>53</b>
<b>APPENDIX C</b>	<b>POST PROCESSING DATA USING DYNAMIC</b>	<b>54</b>
	Input File	54
	Output File naming convention	54
<b>C.1</b>	<b>Setting up the Dynamic Processing Directory</b>	<b>55</b>
	Model configuration file	56
	Model 6 configuration file	56
	Model 7 configuration file	57
	Model 10 configuration file	57
<b>APPENDIX D</b>	<b>ACCELEROMETERS</b>	<b>59</b>

## TABLE OF FIGURES

FIGURE 1. GROUND EFFECT IS ENCOUNTERED BY AN AIRPLANE OPERATING WITHIN A SEMISPAN OF THE GROUND.	7
FIGURE 2. DIAGRAMS OF THREE RESEARCH PLANFORMS.	9
FIGURE 3. DYNAMIC GROUND EFFECT MODEL SUPPORT CART.	11
FIGURE 4. DATA ACQUISITION SYSTEM FOR DYNAMIC GROUND EFFECT TEST.	12
FIGURE 5. ACCELEROMETER LAYOUT FOR TU-144 PLANFORM.	16
FIGURE 6. ACCELEROMETER LAYOUT FOR TCA PLANFORM.	17
FIGURE 7. COMPARISON OF STATIC LIFT CURVES FOR THE ELLIPTICAL WING PLANFORM WITH THOSE IN CURRENT LITERATURE.	22
FIGURE 8. EFFECTS OF VARIOUS SINK RATES ON DYNAMIC GROUND EFFECT FOR THE TU-144 PLANFORM.	23
FIGURE 9. EFFECTS OF VARIOUS SINK RATES ON DYNAMIC GROUND EFFECT FOR THE TCA PLANFORM AT $\alpha = 9$ DEGREES.	24
FIGURE 10. EFFECTS OF VARIOUS SINK RATES FOR THE TU-144 PLANFORM.	24
FIGURE 11. EFFECTS OF VARIOUS SINK RATES ON DYNAMIC GROUND EFFECT FOR THE ELLIPTICAL WING.	25
FIGURE 12. ELAPSED TIME ASSOCIATED WITH RUNS AT VARYING SINK RATES.	26
FIGURE 13. INERTIAL LOAD REMOVAL FOR NORMAL FORCE IN A DYNAMIC RATE, SINK RATE = -4.667 FT/SEC.	27
FIGURE 14. SPECTRAL ANALYSIS OF DYNAMIC RUN.	28
FIGURE 15. COMPARISON OF DYNAMIC AND STATIC GROUND EFFECT LIFT CURVES FOR TU-144 MODEL.	29
FIGURE 16. COMPARISON OF DYNAMIC AND STATIC GROUND EFFECT LIFT CURVES FOR TCA PLANFORM.	29
FIGURE 17. COMPARISON OF DYNAMIC AND STATIC GROUND EFFECT LIFT CURVES FOR ELLIPTICAL WING PLANFORM.	30
FIGURE 18. COMPARISON OF FLIGHT AND WIND TUNNEL DATA FOR TU-144.	30
FIGURE 19. INCREMENTAL LIFT COEFFICIENT VERSUS ASPECT RATIO FOR STATIC AND DYNAMIC GROUND EFFECT MEASURED IN THE WIND-TUNNEL AT $H/B=0.3$ .	31
FIGURE 20. INCREMENTAL LIFT COEFFICIENT VS ASPECT RATIO FOR STATIC AND DYNAMIC GROUND EFFECT MEASURED IN THE WIND-TUNNEL AT $H/B=0.3$ .	32

## Introduction

The development of supersonic transport aircraft with slender wing configurations introduces increasingly sophisticated flight control requirements for the improvement of landing and takeoff performance. The future of the aerospace industry lies in meeting the demands for improved performance and reliability in aircraft and doing this in less development time and at lower costs. The conceptual and design phases play an important part in determining the airplane program cost.<sup>1</sup> Correctly identifying configuration deficiencies during the preliminary design of the aircraft can reduce both the development time and the cost of the airplane. Accurately predicting the landing characteristics of the airplane is an important ingredient of the preliminary design phase.

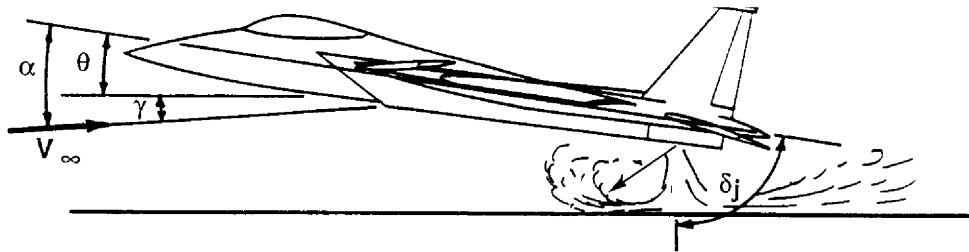


Figure 1. Ground effect is encountered by an airplane operating within a semispan of the ground.

“Ground effect” is the phenomenon encountered when an aircraft nears the ground during either a landing or takeoff. When the aircraft operates within a semispan of the ground, incremental forces develop due to the interaction of the flow field with the ground. At low lift levels ( $C_L < 2$ ) this aerodynamic effect is generally characterized by an increase in the lift curve slope, a decrease in induced drag, and an increase (nose up) in the airplane pitching moment.<sup>2</sup> For low aspect-ratio aircraft, ground effect can severely affect the pilot’s landing performance.<sup>3</sup> Ground effect is a design driver of the landing gear, high lift devices, stability and control system, and if present the thrust vectoring system.

In the past, ground effect was studied as a steady-state situation in which incremental changes to aerodynamic forces and moments were determined. The prominent method of predicting ground effect was to statically place the configuration at progressively shallower heights above a ground plane, taking data at each height. Distinct differences between data obtained from steady-state wind-tunnel testing and dynamic flight data for low-aspect ratio aircraft have been documented.<sup>4</sup> Comparisons of static and dynamic ground effect tests show a trend for over predicting the lift close to the ground for static data for highly swept, low aspect ratio aircraft. These same trends can be seen in lift, drag and pitching moment. Since an aircraft in flight approaches the ground dynamically, any overestimation of this effect by a set of static data may result in undersized aerodynamic flight control surfaces.

In recent years, a variety of innovative testing concepts dealt with the difficulties inherent in obtaining adequate experimental data in a dynamic situation. In references 3, 9, and 10, wind

tunnel data were obtained while moving the sting-mounted model vertically to the ground plane. Data were limited to constant rates of descent for a given run. In references 11, 14, the model was moved horizontally through a static test chamber towards an inclined plane and data were limited to a constant glide path angle. During typical flight landings, the portion of flight influenced by ground effect is characterized by continuously varying sink rate and glide path angles. Keeping conditions constant in each approach becomes more difficult as the model approaches the ground, which coincides with the measurement period when ground effect becomes most significant.

The measurement process is equally challenging for flight testing where flight safety becomes an issue and the airplane must be operated within a small range of vertical and horizontal velocities whenever it is in close proximity to the ground. In addition, flight testing is becoming increasingly expensive and can only be performed after the aircraft has been built.

In the October 1997 Dynamic Ground Effect (DGE) Test, emphasis was placed on improving accuracy of the ground effect data by using a “dynamic” technique in which the model’s vertical motion was varied automatically during wind-on testing. This report describes and evaluates different aspects of the dynamic method utilized for obtaining ground effect data in this test. Three models, the Technical Configuration Aircraft (TCA), the TU-144, and the Elliptical wing planform with a NACA 0012 airfoil, were tested modifying external conditions incrementally. The methodology used for acquiring and processing time data from the dynamic ground effect wind tunnel test is described. Balance force and moment data measuring aerodynamic forces on the model, contain significant inertial loads due to sting motion and support dynamics. Normal accelerations were measured and used to correct these balance forces. This work addresses the method of correction to the balance loads developed on this data.

## Experimental Approach

To investigate the effects of low aspect ratio and sweep angle on ground effects, three research models were tested: (1) an elliptical wing with a NACA 0012 airfoil, (2) a TU-144 wing with a biconvex airfoil and (3) and a Technical Configuration Aircraft (TCA) planform with a biconvex airfoil. The two HSCT Models (the TU-144 and the TCA) were uncambered wings and featured trailing edge flaps deflected 10 degrees.

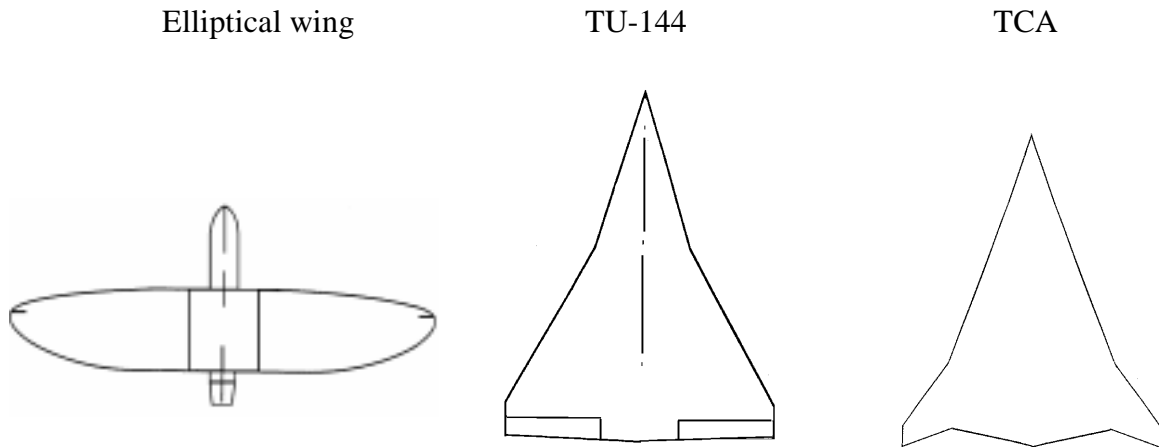


Figure 2. Diagrams of three research planforms.

The Elliptical wing planform has an aspect ratio of 7 and an unswept leading edge. With the highest lift-curve slope of the models, it was used for determining the static flow angularity as a function of ground height. Previously used in other experiments in the same wind tunnel, this model provided lift curve comparisons to validate the technique. The TU-144 planform, with an aspect ratio of 1.6, was used for correlating wind tunnel data to that taken in flight test, and for validation of the wind tunnel as a way of acquiring quality DGE data with parametric variations. The TCA planform, with an aspect ratio of 2, was used to investigate the extent to which DGE reduces lift below that in static ground effect.

The models were rigidly mounted on a sting in the wind tunnel by means of a force balance and were restrained in all directions of motion. Model movement and position were computer controlled with the capability of performing coordinated vertical travel and pitch. The test plan consisted of lowering the model to the ground at varying sink rates and angles of attack while measuring ground effect through lift and pitching moment measurements.

All models were symmetrical airfoils with the same structure consisting of an aluminum plate sandwiched by wood pieces and surrounded by a fiberglass cloth cover. Each model utilized the same VST-2 balance for support and shared a common specially designed upper surface mounted balance adapter. Table 1 presents configurational features for each model. The airfoil thickness varied from approximately 2" near the balance to being very thin at the airfoil edges. The models have a round leading edge (leading edge radius = 0.05") and a sharp trailing edge made of aluminum.

Model #	Planform	$\Lambda_{\text{Inboard}}$ (deg)	$\Lambda_{\text{Outboard}}$ (deg)	AR	b (in)	S (ft <sup>2</sup> )	Mass (slgs)
6	TCA wing	71	52	2.03	48.0	7.89	1.74
7	TU-144 wing	76	57	1.64	47.1	9.45	1.85
10	Elliptical wing	0	0	7.00	80.62	6.45	4.49

Table 1. Physical properties of three basic planforms.

The Test Facility was NASA Langley's 14-by 22- Foot Subsonic Wind Tunnel consisting of a Model Preparation Area (MPA) and a closed-circuit, single-return, atmospheric wind tunnel. The MPA is a large enclosed high bay used for model setup, checkout, and test. Models were installed on a mobile cart in the MPA and moved into the wind tunnel test section fully assembled and calibrated.

The wind tunnel closed test section is 14.5 ft high by 21.75 ft wide by 50 ft long and was configured with walls and ceiling in place for this test. The test section floor is composed of two removable floor sections which were replaced with the dynamic cart configured for model support. Visual access into the test section was provided by television cameras located at various positions in the test chamber.

A floor boundary-layer removal system at the entrance to the test section was in place for the ground-effects testing. Floor boundary layer control was provided by a suction device ahead of the front cart. The boundary-layer removal system consists of a blower and 900-hp drive motor, a suction plenum chamber, interconnecting ducts and control valves.

Models were installed on the Dynamic Ground Effect Mobile Cart and moved into the wind tunnel section fully assembled and calibrated on four air-bearing assemblies. The cart was raised into the front test bay by hydraulic lifts becoming the floor of the test section. Powered by a 5,000 psi hydraulic system, the cart is capable of producing vertical velocities up to 15 feet/sec maintained to within 12 inches of the floor and pitch angular rates up to 60°/sec. The model can be pitched from -10° to 50° and yawed ±15°. Model movement and position are computer controlled with the capability of performing coordinated vertical travel and pitch.

## DYNAMIC MODEL SUPPORT SYSTEM

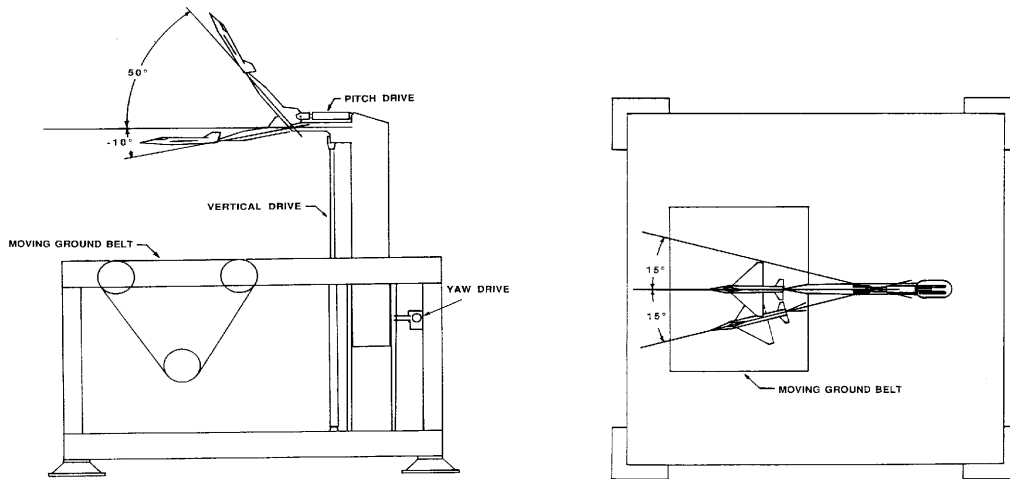


Figure 3. Dynamic Ground Effect model support cart.

The HS-12 sting system was designed so that the end of the sting attached directly to the balance. Angle-of-attack ranges other than that from  $\pm 15$  degrees were obtained with an angle section referred to as a “knuckle”. The sting was stiffened in the longitudinal plane of symmetry and had 4 degrees of upward bend approximately 2 feet downstream of the balance attachment joint. A sting adapter was designed and fabricated to fit between the model sting and the balance. The adapter was needed to get high-lift approach alphas as close to the ground plane without pitching the model/sting system up and away from the ground plane.

Two types of tests were conducted in the 14- by 22- Foot Tunnel: (1) static tests where time-averaged data were of primary concern, and (2) dynamic tests where time-dependent data were of primary concern. In both cases, a single data system was used. The data acquisition system (DAS) consisted of a model interface (MIF) cabinet, input/output (I/O) peripherals, and two ModComp Classic 9250 computers. One computer was dedicated to the wind tunnel and the other to the MPA. A data cable plugboard cabinet routed data from the various test sites to the appropriate data acquisition subsystems.<sup>5</sup> On-line data processing during the test provided the test engineer with information needed to direct the research investigation. Each run was predetermined to have an 8-second duration at a sampling frequency of 150 Hertz per channel.

# DGE DATA ACQUISITION

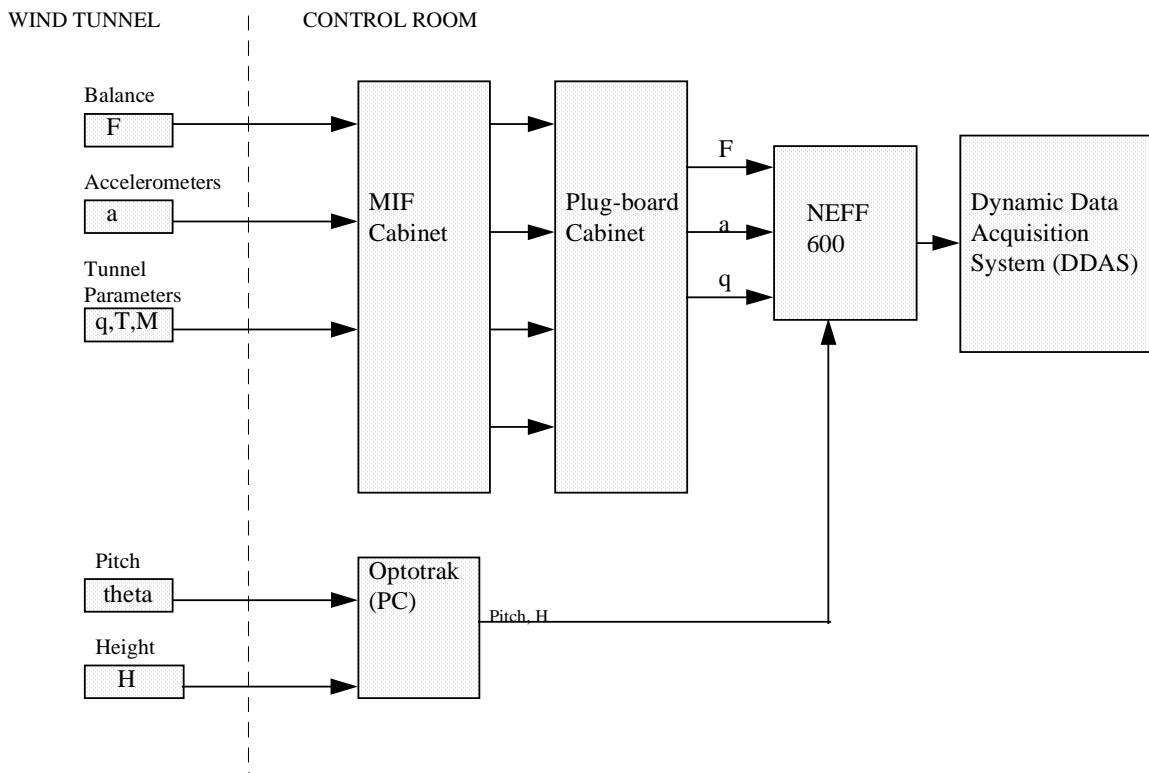


Figure 4. Data acquisition system for dynamic ground effect test.

Instrumentation wiring was routed from the model through the model support system to a model interface (MIF) console located beneath the test section. Each MIF contains a Neff 600 analog signal conditioner, a digital interface and a tachometer interface. The MIF rack provided an interface between the wind tunnel model instrumentation and the data acquisition system in the 14- by 22-Foot Subsonic Tunnel. In addition, the MIF cabinet provided regulated direct current (DC) for the model instrumentation.

Analog signal conditioning was provided for the analog measuring devices by a Neff 600 analog signal conditioner. The output signals from the Neff were amplified, converted to digital codes, recorded and directly processed. Analog and digital input data were transmitted from the test sites on the MPA to a plugboard cabinet in the control room. Analog data were patched 16 channels at a time while digital data were patched, 8 multiplexed channels at a time. A ModComp 9250 computer was used for the acquisition and archival of all data. Model instrumentation was connected to the data acquisition system via the MIF console.

Each test was conducted at constant dynamic pressure or velocity. The dynamic pressure in the test section was monitored by using both a static pressure probe located 12 feet upstream of the

test section and a total pressure probe located 59.4 feet upstream of the test section in the settling chamber. The static and total pressure probes were connected to a differential, fused-quartz bourdon pressure transducer with a digital readout. This transducer has a measured accuracy of  $\pm 0.08$  psf of the full-scale reading. The differential pressure reading between the static and total pressure readings is referred to as the indicated dynamic pressure,  $q_{ind}$ . This indicated dynamic pressure is related to the actual dynamic pressure of the test section by means of calibration curves that have been determined for the different test-section configurations. No wall corrections were implemented in the code. The test was run with the boundary layer removal system in place. A test Reynolds number of approximately  $7 \times 10^6$  and Mach  $\approx 0.24$  was maintained by adjusting the tunnel speed.

## **Instrumentation**

During the dynamic test, vibrations from the driving system were introduced into the measured loads of the system. Accelerations on the model were measured and used to correct balance forces. The vibrations were removed by measuring the accelerations of the system, calculating the inertial loads from these accelerations, and then subtracting the inertial loads from the balance forces.

Actual forces and moments were obtained by correcting all balance component test data for the applicable component interaction data that were recorded during the balance calibration. Force and moment measurements were made using the VST2 six component strain gauge balance. The VST2 has a calibration range of  $\pm 1000$  pounds in the normal direction,  $\pm 500$  pounds in the axial direction,  $\pm 4000$  in-pounds of pitching moment,  $\pm 3000$  in-pounds of rolling moment,  $\pm 3000$  in-pounds of yawing moment, and  $\pm 500$  pounds in the side direction. Interactions between the components were accounted for using a  $6 \times 27$  matrix provided with the balance.

An Optotrak System measured pitch angle and height above the ground. Two cameras were set up in the ceiling of the wind tunnel to view six infrared diodes on the model. These markers or strobers provided height (above ground plane) and the model pitch angle measurements. A Pentium based PC having a 2-channel I/O card provided the data acquisition for the system. The PC based system provided a sampling rate of approximately 50 samples/sec for each channel. Synchronization was provided between this system and the ModComp through a system of interrupts initiated by the ModComp. The ModComp provided integration of the data packets originating from the Optotrak, i.e., for two channels of data (pitch and height) into the database to be archived.

Six Endevco model 7290A-10 accelerometers were used to measure model accelerations. These accelerations have a range of  $\pm 10$  g and a frequency response of 0 to 500 Hz. The accelerometers were positioned in an orthogonal layout on the models, as shown in Figures 5 and 6.

## Measurement Technique

The basis for this analysis and computation of the unsteady motion of a flight vehicle is to treat the model of the vehicle as a single rigid body with six degrees of freedom. The mathematical model is simplified further by treating Earth as flat and stationary in inertial space. The rigid body equations are derived by applying Newton's laws to an element of the model and calculating the summation of all the forces that act upon all the elements in the model. The equation relates the resultant external aerodynamic force on the model to the motion of the reference center.

### *Force and Moment Data Translation*

Moments and forces measured by the balance were translated to the moments and forces acting on the model using equations from Gainer and Hoffman:<sup>6</sup>

X-axis

$$AF_{Model} = -AF_{Balance} \quad (1)$$

$$RM_{Model} = RM_{Balance} + SF_{Balance} \cdot \bar{Z} - NF_{Balance} \cdot \bar{Y} \quad (2)$$

Y-axis

$$SF_{Model} = SF_{Balance} \quad (3)$$

$$PM_{Model} = PM_{Balance} - AF_{Balance} \cdot \bar{Z} + NF_{Balance} \cdot \bar{X} \quad (4)$$

Z-axis

$$NF_{Model} = -NF_{Balance} \quad (5)$$

$$YM_{Model} = YM_{Balance} + AF_{Balance} \cdot \bar{Y} - SF_{Balance} \cdot \bar{X} \quad (6)$$

These equations can be greatly simplified if the model center of gravity is driven to the moment center of the balance (i.e., if  $\bar{X} = \bar{Y} = \bar{Z} = 0$ ).

### Equations for Removal of Inertial Loads

Data obtained from dynamic wind tunnel testing were reduced using the general equations of motion for six degrees of freedom.<sup>7</sup> The equations given here are specialized cases of the general forms given in Gainer and Hoffman's reference. Those equations applied to this test procedure are:

X-axis

$$AF_{Aero} = m(\underbrace{\dot{u}}_1 + \underbrace{qw - rv}_2) + \underbrace{mg \sin \theta}_3 - \underbrace{AF_{Model}}_4 \quad (7)$$

$$RM_{Aero} = \underbrace{\dot{p}I_x}_1 + \underbrace{qr(I_z - I_y) - (pq + \dot{r})I_{xz}}_2 - \underbrace{RM_{Model}}_4 \quad (8)$$

Y-axis

$$SF_{Aero} = m(\underbrace{\dot{v}}_1 + \underbrace{ru - pw}_2) + \underbrace{mg \cos \theta}_3 - \underbrace{SF_{Model}}_4 \quad (9)$$

$$PM_{Aero} = -\underbrace{\dot{q}I_y}_1 + \underbrace{pr(I_x - I_z) + (p^2 - r^2)I_{xz}}_2 - \underbrace{PM_{Model}}_4 \quad (10)$$

Z-axis

$$NF_{Aero} = m(\underbrace{\dot{w}}_1 + \underbrace{pv - qu}_2) - \underbrace{mg \cos \theta}_3 - \underbrace{NF_{Model}}_4 \quad (11)$$

$$YM_{Aero} = \underbrace{\dot{r}I_z}_1 + \underbrace{pq(I_y - I_x) + (qr - \dot{p})I_{xz}}_2 + \underbrace{YM_{Model}}_4 \quad (12)$$

The equations derived in the preceding sections are valid for any orthogonal axes fixed in the model. The models are assumed to be exactly symmetrical about the XZ plane. These equations are limited to models symmetric about the XZ plane, models with no thrust and no change in the mass of the model. Inertial load corrections were performed in two stages with the primary and secondary corrections indicated with numbers 1,2 respectively. The terms numbered 3 were the corrections made by wind off zero and weight tare calibrations. Terms numbered four are the forces and moments measured on the model after a translation from the balance forces and moments.

### Accelerometer Layout for TU-144 (Bottom View)

Distances from MRC to Center of Each Accelerometer (in inches)

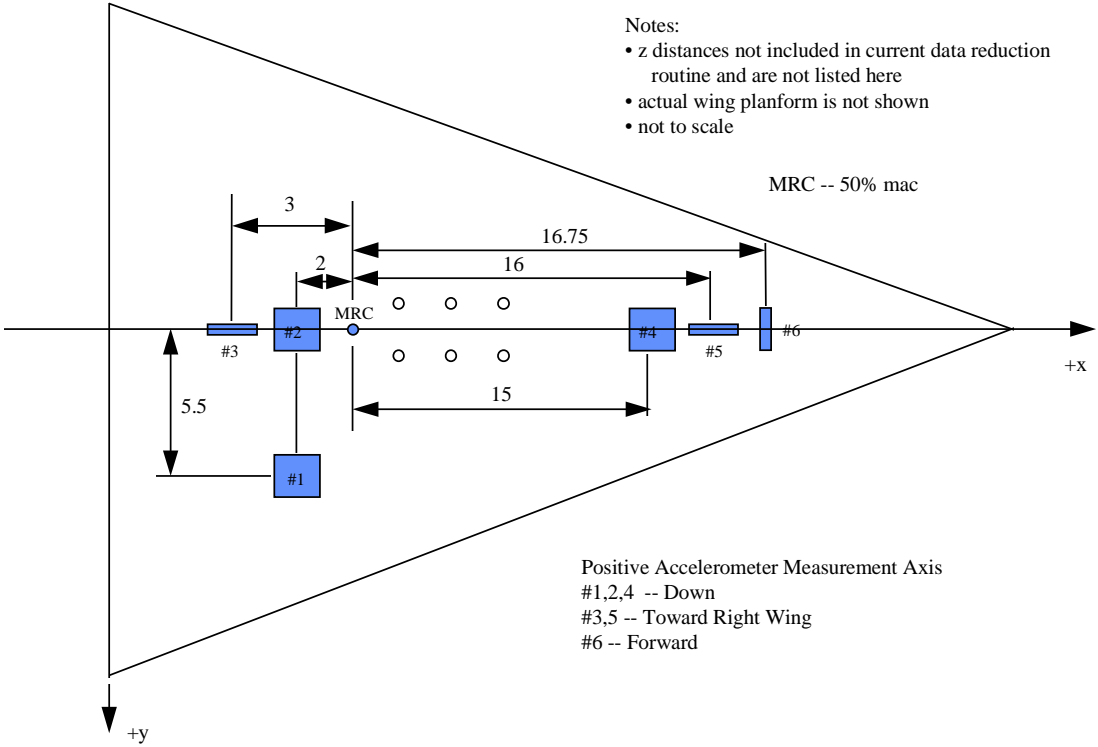


Figure 5. Accelerometer Layout for TU-144 Planform.

### Accelerometer Layout for TCA (Bottom View)

Distances from MRC to Center of Each Accelerometer (in inches)

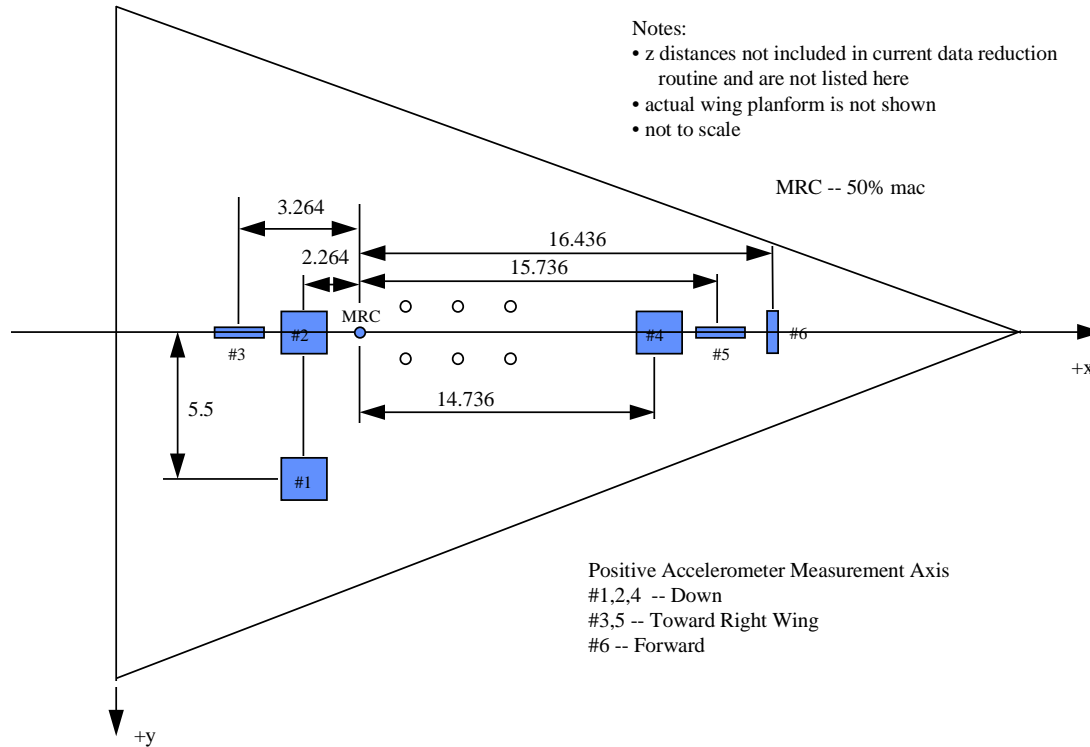


Figure 6. Accelerometer Layout for TCA Planform.

### ***Linear Accelerations***

Accelerometer measurements were combined to calculate linear and angular accelerations. The accelerations were then integrated providing the velocity calculations. Detailed descriptions of these calculations are presented in the following sections.

Axial acceleration, x-axis

$$\dot{u} = A6 - a_{woz} - 1g(\sin \theta) \quad (13)$$

Side acceleration, y-axis

$$\dot{v} = A3 + \frac{A5 - A3}{|xdist5| + |xdist3|} |xdist3| - a_{woz} \quad (14)$$

Normal acceleration, z-axis

$$\dot{w} = A2 + \frac{A4 - A2}{|xdist4| + |xdist2|} |xdist2| - a_{woz} - 1g(1 - \cos \theta) \quad (15)$$

### ***Angular Accelerations***

Roll angular acceleration

$$\dot{p} = \frac{A2 - A1}{|ydist1| + |ydist2|} \quad (16)$$

Pitch angular acceleration

$$\dot{q} = \frac{A4 - A2}{|xdist2| + |xdist4|} \quad (17)$$

Yaw angular acceleration

$$\dot{r} = \frac{A5 - A3}{|xdist3| + |xdist5|} \quad (18)$$

### ***Velocity Calculations***

Velocities in the equations were calculated using a numerical integration scheme based on Tick's rule<sup>8</sup>. The method uses a linear combination of the acceleration time samples ( $a_n$ ) where the  $a_n$  are the integrand values and the  $v_n$  are the integral values. The formula is (using  $v_0 = 0$ )

$$v_{n+1} = v_{n-1} + h(0.3584a_{n+1} + 1.2832a_n + 0.3584a_{n-1}) \quad (19)$$

In the presence of noise, usually associated with high frequencies, this function did not perform well and an alternate method of computation for was used,

$$w = u \cos\theta \quad (20)$$

### ***Sink Rate Calculation***

$$\dot{h} = \frac{w}{\cos\theta} \text{ (ft/sec)} \quad (21)$$

### ***Total Velocity Calculation***

$$V_{Tot} = \sqrt{(V_{Tun})^2 + (\dot{h})^2} \text{ (ft / sec)} \quad \text{where } V_{un} = \text{VELU parameter} \quad (22)$$

### ***Calculated ground height, h/b***

$$\frac{h}{b} = \frac{HGTOPT}{b} \quad (23)$$

### ***Flight Path Angle***

$$\gamma = \tan^{-1}\left(\frac{\dot{h}}{V_{Tot}}\right)(\text{deg}) \quad (24)$$

### ***Angle of Attack***

$$\alpha = \theta - \gamma \quad (25)$$

### ***Corrected Dynamic Pressure***

$$q_{corr} = q\left(\frac{V_{Tot}}{V_{in}}\right)^2 \quad (\text{lbs} / \text{ft}^2) \quad (26)$$

Note that the corrected dynamic pressure measurement was not used in these calculations to conform with the static data reduction which was reduced using the QU parameter.

### ***Corrected Force/Moment Coefficients***

The normal-force coefficient, corrected for inertial loads is

$$C_{N_{corr}} = \frac{NF_{Aero}}{q_{corr}S} \quad (27)$$

The axial force coefficient, corrected for inertial loads is

$$C_{A_{corr}} = \frac{AF_{Aero}}{q_{corr}S} \quad (28)$$

The pitching moment coefficient corrected to the model reference center and for inertial loads is

$$C_{M_{corr}} = \frac{PM_{Aero}}{q_{corr} S \bar{c}} \quad (29)$$

### ***Performance Coefficients***

The calculated lift coefficient,  $C_L$  is defined to be

$$C_L = C_{N_{corr}} \cos \alpha - C_{A_{corr}} \sin \alpha \quad (30)$$

The calculated drag coefficient,  $C_D$  is defined to be

$$C_D = C_{N_{corr}} \sin \alpha + C_{A_{corr}} \cos \alpha \quad (31)$$

## Results and Discussion

One of the purposes of testing a model in the wind tunnel is to estimate the aerodynamic forces the full scale vehicle will experience during operation. Distinct differences between data obtained from steady-state wind-tunnel testing (constant height above ground) and dynamic flight data (descending to the ground) were documented during a series of flight tests of low-aspect ratio aircraft beginning in the late 1960s.<sup>9</sup> Subsequent wind-tunnel experiments in which the dynamic conditions of descending flight were simulated verified this distinction.<sup>10,11,12</sup> The distinction has also been confirmed through recent flight testing which has identified trends dependent on sink rates.<sup>13,14</sup> The development of a ground-based technique at NASA for the measurement of dynamic or time-dependent ground effects was driven by the existence of these large discrepancies between flight test data and conventional wind tunnel ground effects tests for supersonic transport aircraft with high swept wing configurations. The experiment was designed to test the hypothesis that aspect ratio or sweep angle along with rate of descent might be an important parameter in determining actual ground effects. Because ground effects tend to be more significant for low-aspect ratio aircraft, the current development of high-speed civil transport aircraft which use slender wing configurations has motivated research into this field.

In order to evaluate the dynamic ground effects of low aspect ratio and highly swept wing configurations, the aerodynamic characteristics of an unswept elliptic wing model and two highly swept wing models were tested in the subsonic wind tunnel. The elliptic wing model, which had been used in this same wind tunnel on previous tests, enabled validation of the *test method* by providing comparative data for steady state tests. Results depicting static lift curve data in Figure 7 show good agreement with prior tests for the Elliptical wing planform<sup>15</sup>.

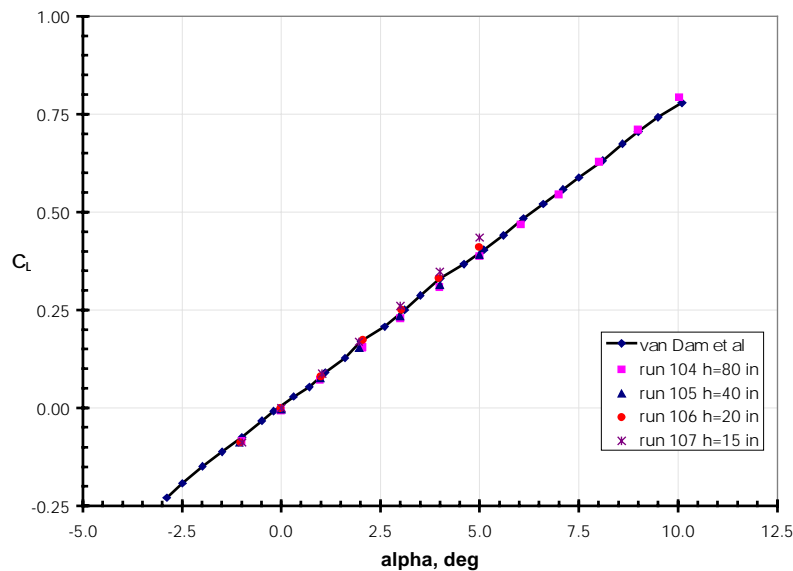


Figure 7 Comparison of static lift curves for the Elliptical wing planform with those in current literature.

An advantage of wind tunnel testing is that conditions can be held constant and varied incrementally in order to isolate different effects and their sources. Comparisons of the effects of sink rate on ground effect for the different planforms are illustrated in Figures 8-11. The fractional increase in the lift coefficient during a plunge (or a descent), normalized to an Out of Ground Effect (OGE) lift coefficient, is depicted for runs at consecutively higher rates of descent. All other conditions during the runs were held constant. The rate of descent was varied as shown from -1, -2.333, and -4.667 ft/sec with the model held at a constant angle of attack of 9, 11 or 5 degrees. The three planforms showed comparable ground effect increases for each sink rate tested. Ground effect increased consistently for all models for the three sink rates.

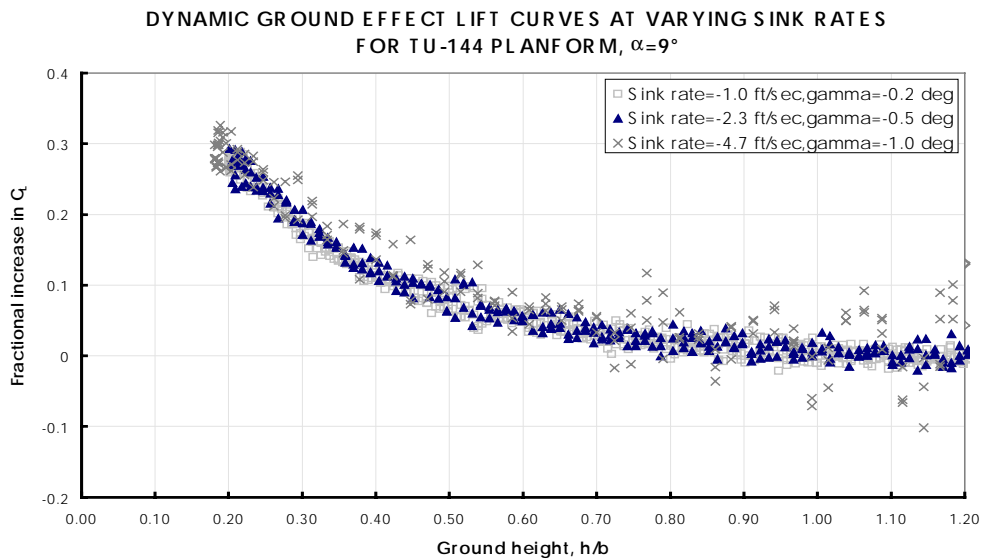


Figure 8. Effects of various sink rates on dynamic ground effect for the TU-144 Planform.

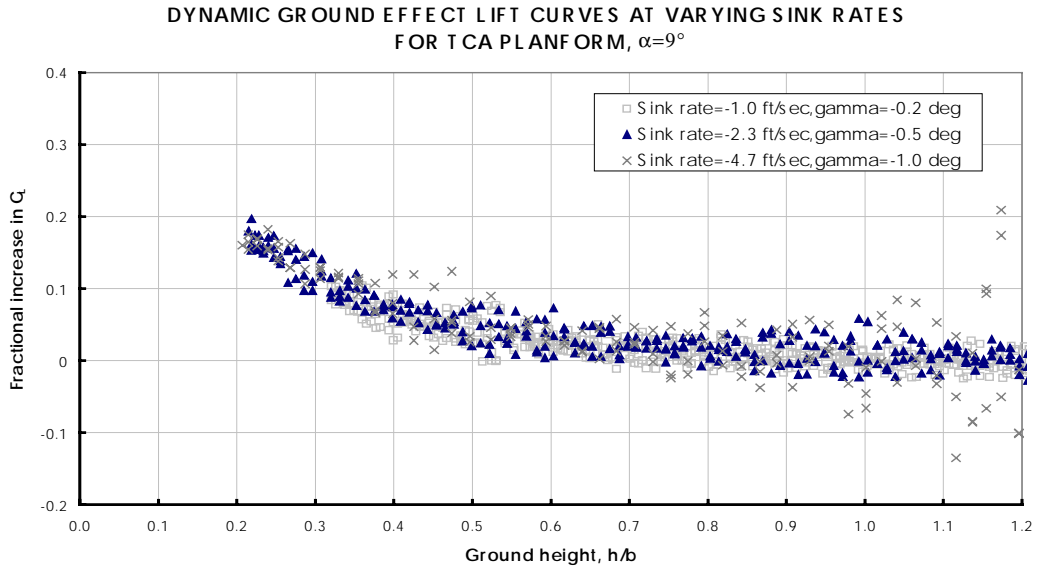


Figure 9. Effects of various sink rates on dynamic ground effect for the TCA planform at  $\alpha = 9$  degrees.

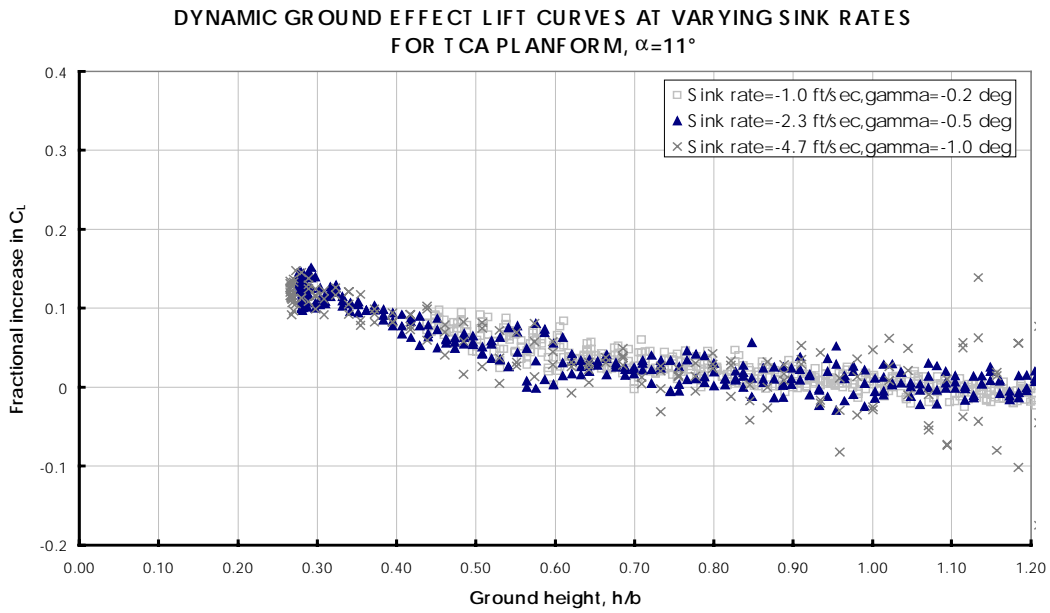


Figure 10 Effects of various sink rates for the TU-144 planform.

DYNAMIC GROUND EFFECT LIFT CURVES AT VARYING SINK RATES FOR  
ELLIPTICAL WING,  $\alpha=5^\circ$

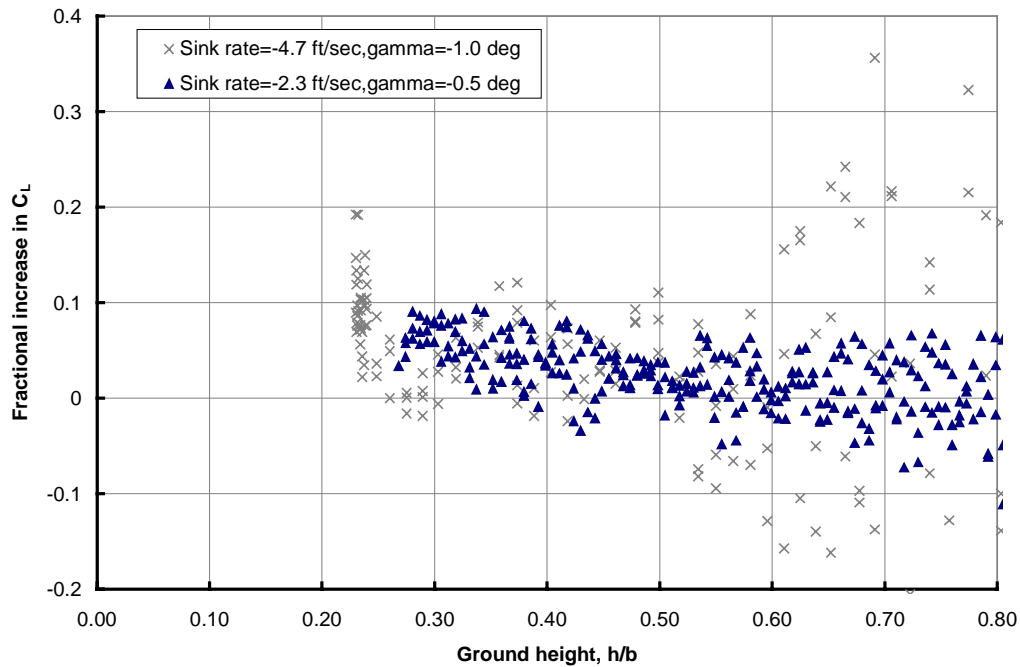


Figure 11. Effects of various sink rates on dynamic ground effect for the Elliptical wing.

Examination of the lift curves in Figures 8-11 shows an increasing dispersion in the fractional lift associated with higher sink rates. To further investigate this scattering, the lift curves for the TU-144 planform were plotted against time and ground height. Figure 12 illustrates the fractional lift on ground approach during an 8 second run for differing sink rates. In each run, the start of the plunge is seen at the top of the graph. Associated with the start of the plunge is the vibration of the driving equipment. Forces related to these vibrations at the start of the plunge have a settling time of approximately 0.8 seconds. For slow sink rates as seen in the top graph, enough time elapses between the plunge and the in ground effect to allow for the settling of these forces. For the higher sink rate, there is no settling time allowing for the decay of these forces before the model is considered to be in-ground effect. This problem can be addressed by either improving the driving mechanism to reduce the impact of the start of the plunge or starting the plunge at a higher ground height (if possible) allowing more time to elapse before the model is in ground effect. For the higher sink rates, more control is required for starting and stopping the equipment smoothly and in a shorter amount of time. This would enable a more constant sink rate on start up and at closer proximity to the ground.

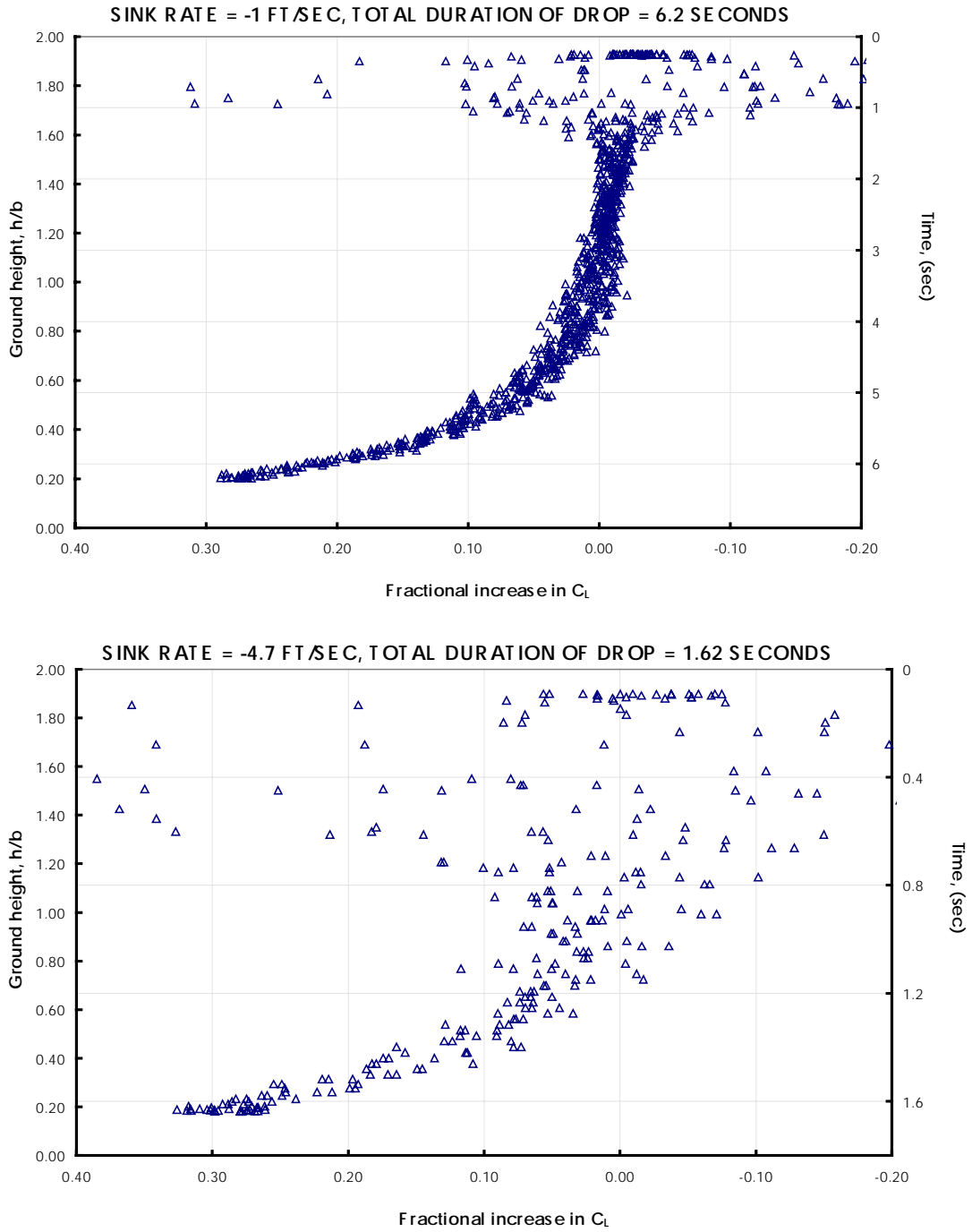


Figure 12. Elapsed time associated with runs at varying sink rates.

In dynamic wind tunnel testing, vibrational loads imparted to the model from the driving system prevent determining aerodynamic data directly from the time data. By measuring the model accelerations, these vibrational loads can be removed from the system.<sup>16</sup> In this wind tunnel test, vibrational loads were either removed or reduced so as to have a negligible effect on the aerodynamic results. Figure 13 illustrates the removal of inertial loads from the normal force measured by the balance during a dynamic run.

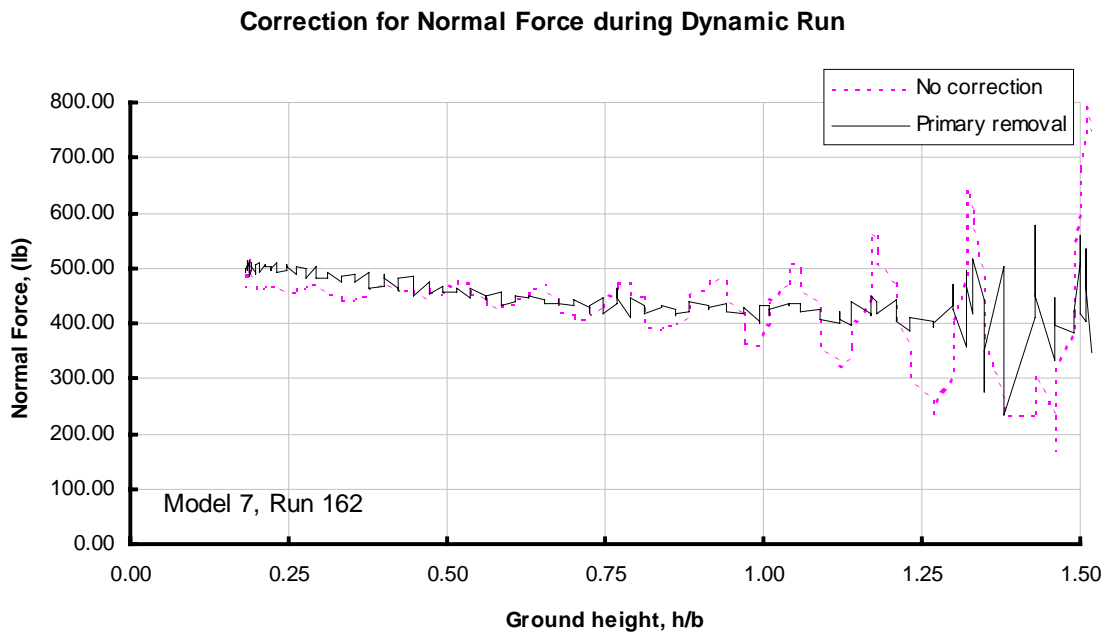


Figure 13. Inertial load removal for normal force in a dynamic rate, sink rate = -4.667 ft/sec.

Small variations remaining in the residual load are attributed to a high frequency noise level apparent in the accelerometer prior to the run as well as small errors in acceleration measurements due to calibration. To study the effect of equipment vibration caused by the *dynamics* of a run on the quality of the data, a spectral analysis of the components of the run pictured in Figure 14 was studied. Frequency components for the normal acceleration, the normal force (before inertial load removal) and the normal force (after correction) are seen in Figure 14. The vibrations at approximate 9 Hz level are reduced while a small amount of high frequency noise (35 Hz) in the acceleration continues to be seen after correction is applied to the normal force.

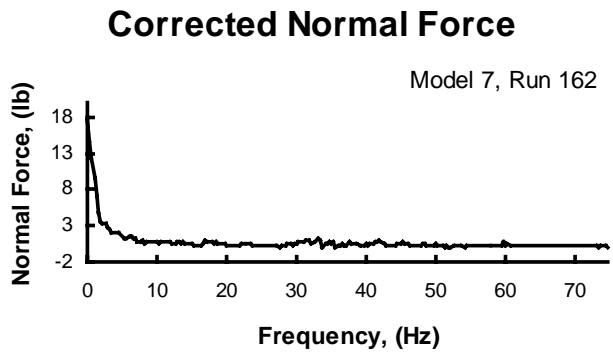
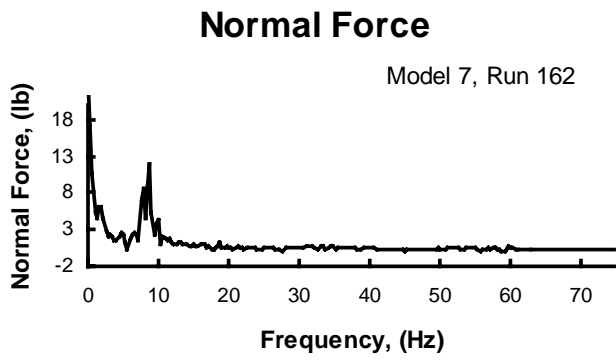
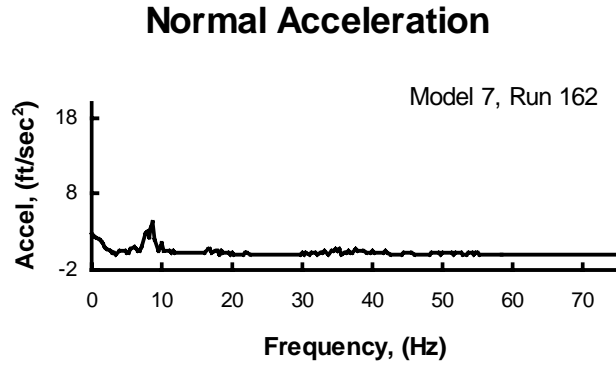


Figure 14. Spectral analysis of dynamic run.

Results presented in Appendix A summarize the removal of inertial loads for normal and axial forces as well as for pitching moment for each model.

Dynamic wind tunnel measured lift increments are presented and compared with steady state wind tunnel data for each planform in Figures 15 through 16 and show a minimal variation which was a characteristic result for this experiment. Data for the static runs are shown to be relatively close to the dynamic results.

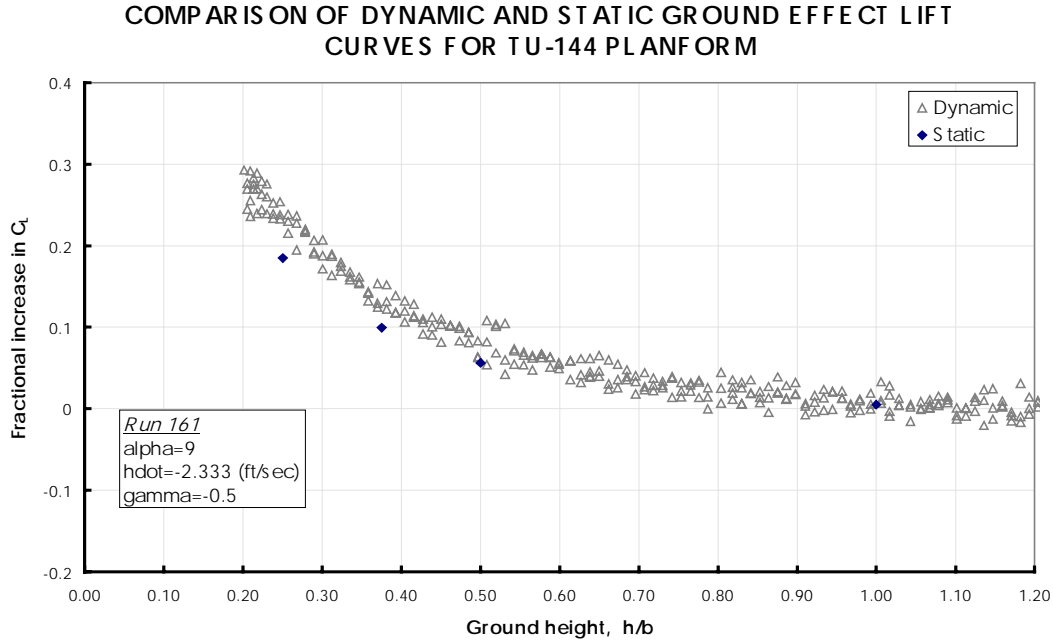


Figure 15. Comparison of dynamic and static ground effect lift curves for TU-144 model.

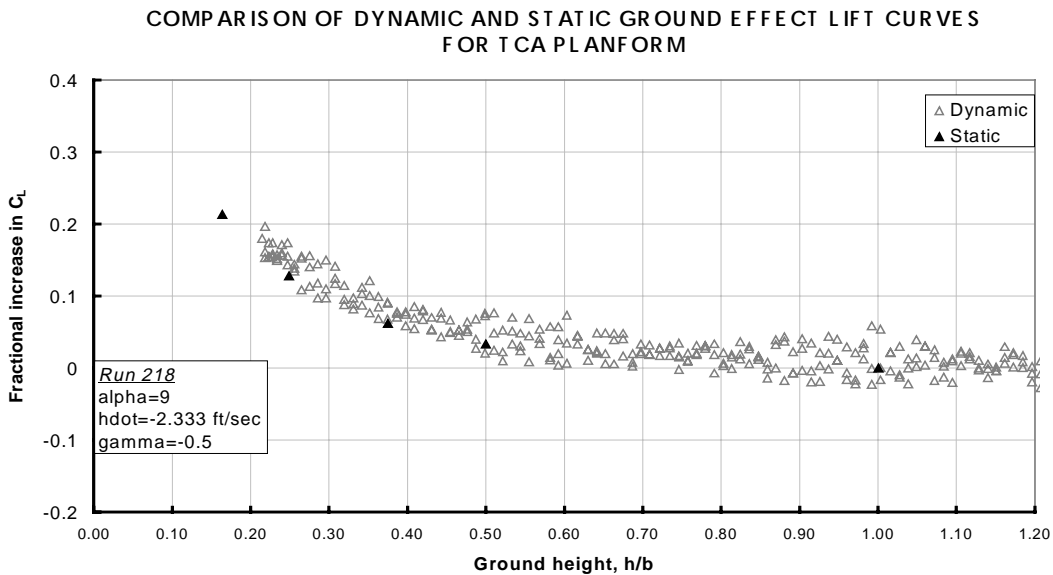


Figure 16. Comparison of dynamic and static ground effect lift curves for TCA planform.

**COMPARISON OF DYNAMIC AND STATIC GROUND EFFECT LIFT CURVES FOR ELLIPTICAL WING PLANFORM**

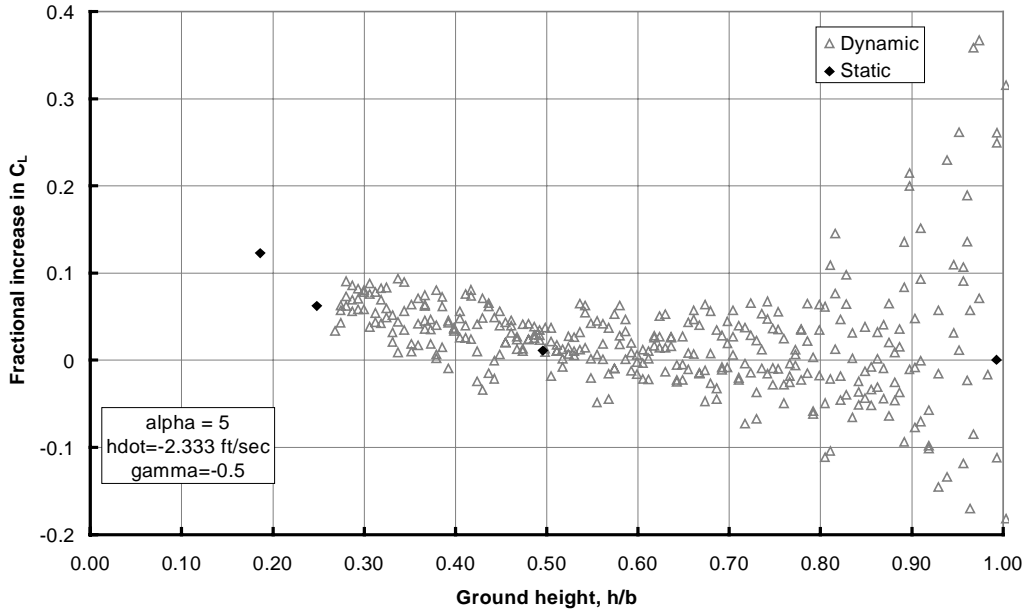


Figure 17. Comparison of dynamic and static ground effect lift curves for elliptical wing planform.

Flight measured increments in lift are presented and compared to dynamic wind tunnel data for the TU-144. Figure 18 demonstrates the close approximation dynamic wind-tunnel data produce to the flight test data.

**Comparison of Flight and Wind Tunnel Data for TU-144**

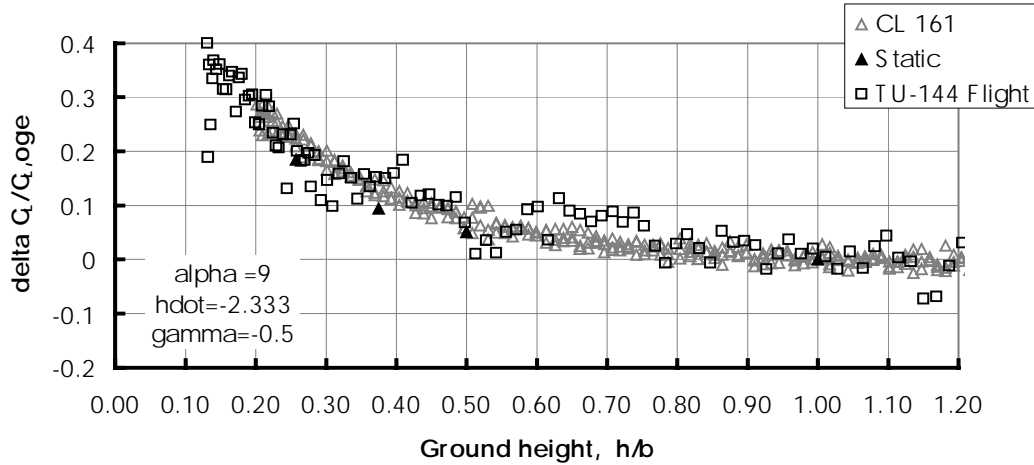


Figure 18. Comparison of flight and wind tunnel data for TU-144.

Figures 19-20 compare the incremental lift coefficient on several airplane configurations having widely different aspect ratios and sweep angles at  $h/b = 0.3$ . Flight data for the TU-144 and the F16-XL were obtained using “constant-alpha-approaches” and a constant throttle setting in Flight Test Maneuvers. Static and dynamic data for the TU-144 and TCA planforms were compared with the University of Kansas data. The large disparity between the static wind-tunnel data and the dynamic and flight test data is not apparent in the Langley data. Static and dynamic data for the Langley models showed a strong correlation with the flight test data.

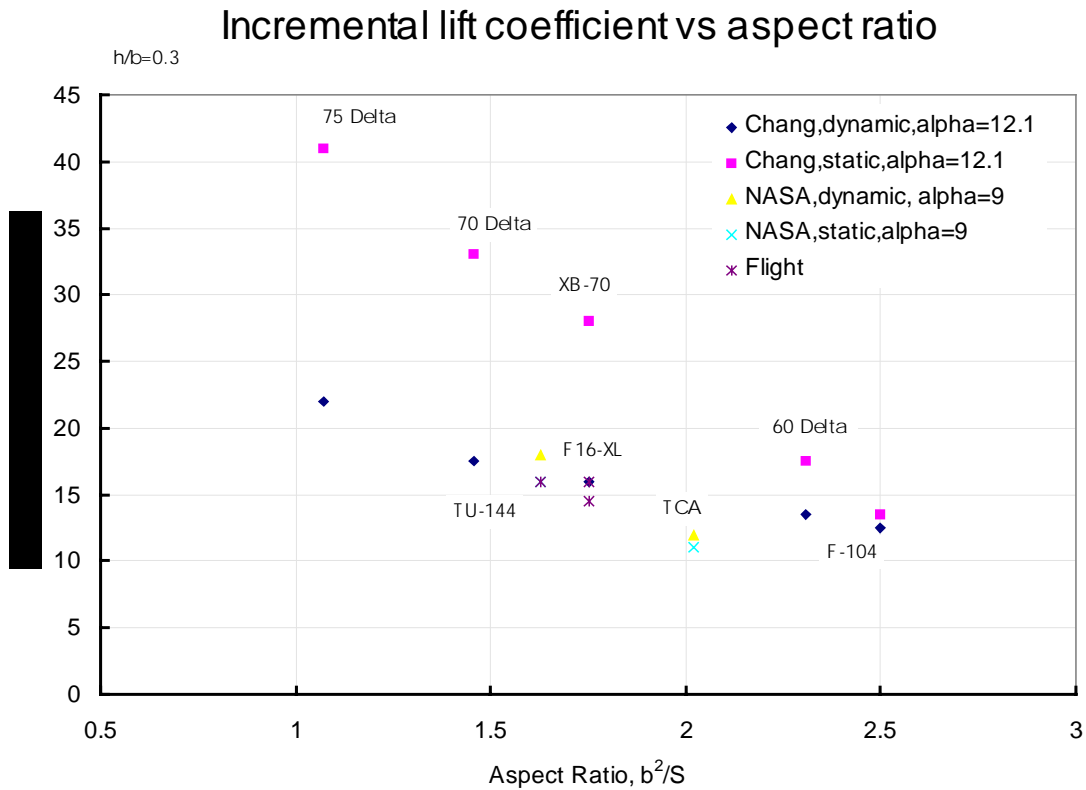


Figure 19. Incremental lift coefficient versus aspect ratio for static and dynamic ground effect measured in the wind-tunnel at  $h/b=0.3$ .

## Incremental lift coefficient vs sweep angle

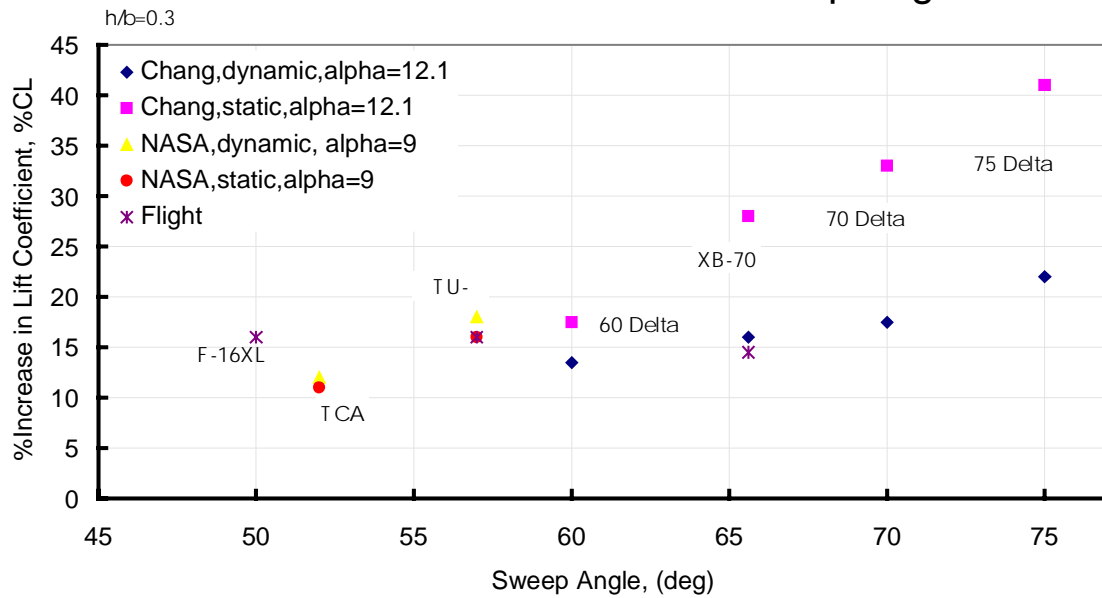


Figure 20. Incremental lift coefficient versus aspect ratio for static and dynamic ground effect measured in the wind-tunnel at  $h/b=0.3$ .

## **APPENDIX A Inertial Loads Removal**

Balance force and moment data for each model in the test facility contained significant inertial loads due to carriage motion and support dynamics. Six accelerometers were placed in an orthogonal layout in order to measure the inertial loads on the model. Prior to a set of runs for each model, a wind-off weight tare and three calibration runs (pitch, yaw, roll) were completed. The weight tare calculated the weight of the model and provided the system with additional correction factors for the weight factor of each model. Extensive data is available from three normal, two axial, and two side accelerometers. This section addresses the method of correction to the balance loads developed on the latest data.

The calibration run consisted of a wind-off, static run during which the model was bumped or “jogged” in one of three directions (pitch, yaw, roll) to induce inertial loads. The model was kept at a constant height of 50” above the ground and at a constant angle of attack. The data set for these runs was curve fitted in linear and multiple regressions for the optimal removal of inertial loads.

Additional calibration was performed for each acceleration in order to remove a bias or zero offset. This was performed by averaging each acceleration over a 0.5 second (75 sample) period at the beginning of each run (prior to any movement of the mast) and using this value as a zero offset which was subtracted out of all remaining samples per acceleration.

Results of the correction for inertial loads are presented for each force and moment. Subtraction of the inertial loads accounted for the removal of most of the measurable vibrational effects. Secondary accelerations from coupled velocity terms (2) in equations 7.0-12.0 had a negligible effect on the removal of inertial loads. For tests without significant model velocities, the correlation between the measured loads and associated accelerations provided a measure of errors in the system. Models 6 and 7 show excellent correlation between either normal or axial loads and corresponding accelerations. A spectral analysis exhibits frequencies associated with the inertial loads. In addition, the spectral analysis pinpoints low level noise (at 1 Hz) and higher frequencies (at 60 Hz) which interfered in some cases with the correction. Small variations remaining in the residual load were attributed to the noise level of the signal as well as errors in acceleration measurements.

- External loads imparted on the system from striking it
- Impulses in the analog signal not resulting from actual loads
- Noise level of the signal
- Errors in acceleration measurements

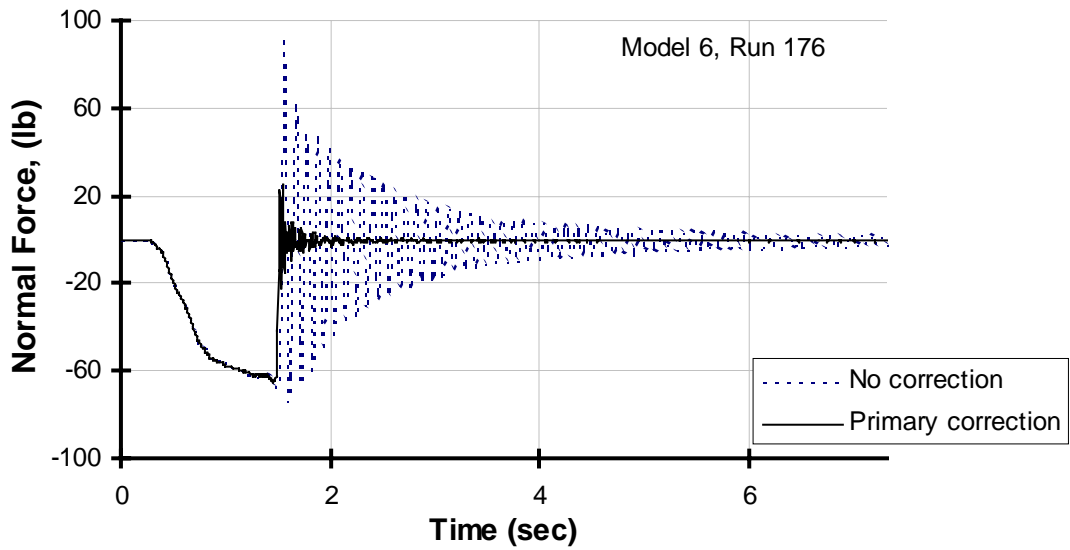


Figure A1. TCA wing inertial loads correction for normal force.

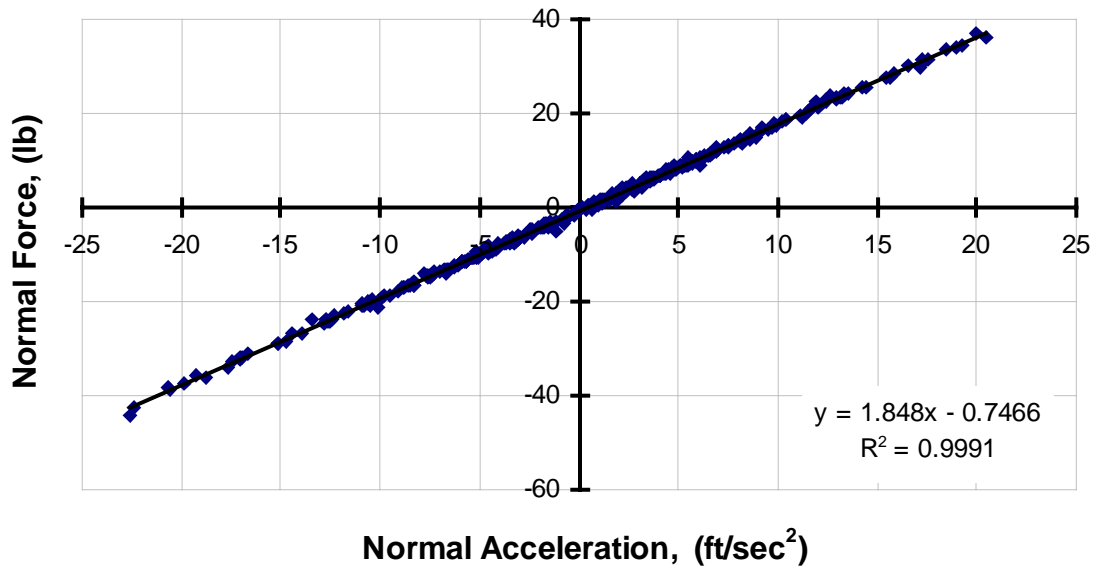


Figure A2. TCA wing correlation between normal force and normal acceleration.

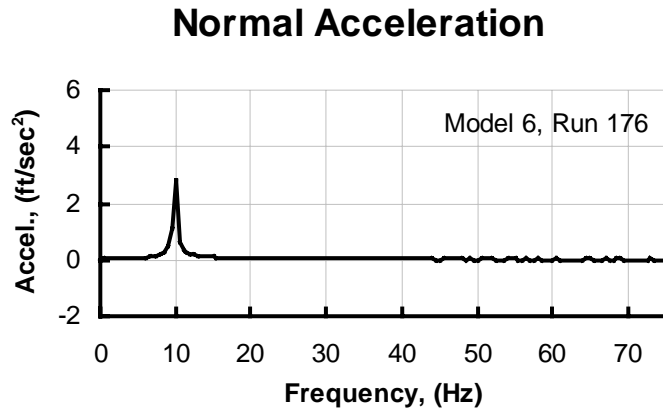


Figure A3. Spectral Analysis of Normal Acceleration.

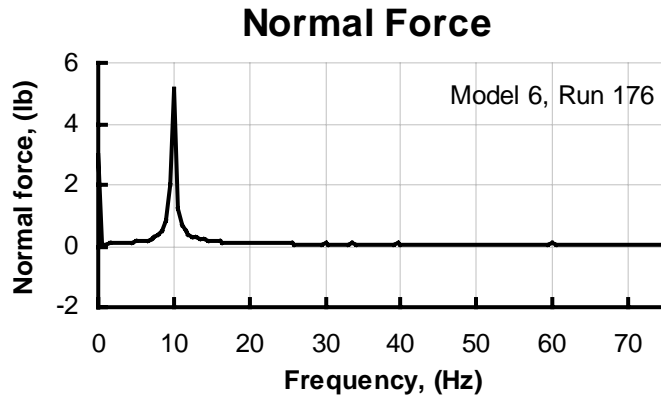


Figure A4. TCA wing Spectral Analysis of Normal Force, no correction.

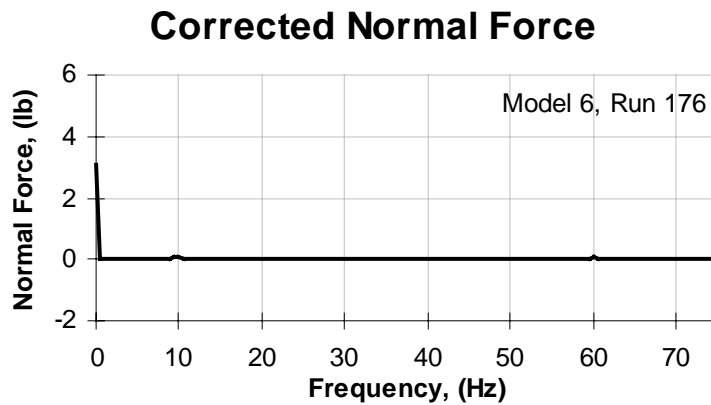


Figure A5. TCA wing Spectral Analysis of Normal Force, primary correction.

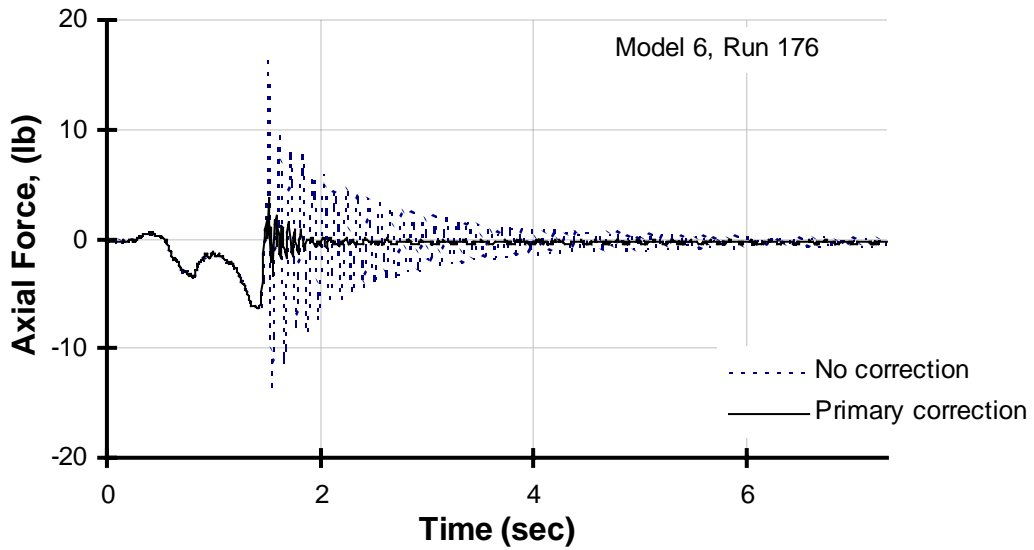


Figure A6. TCA wing inertial loads correction for axial force.

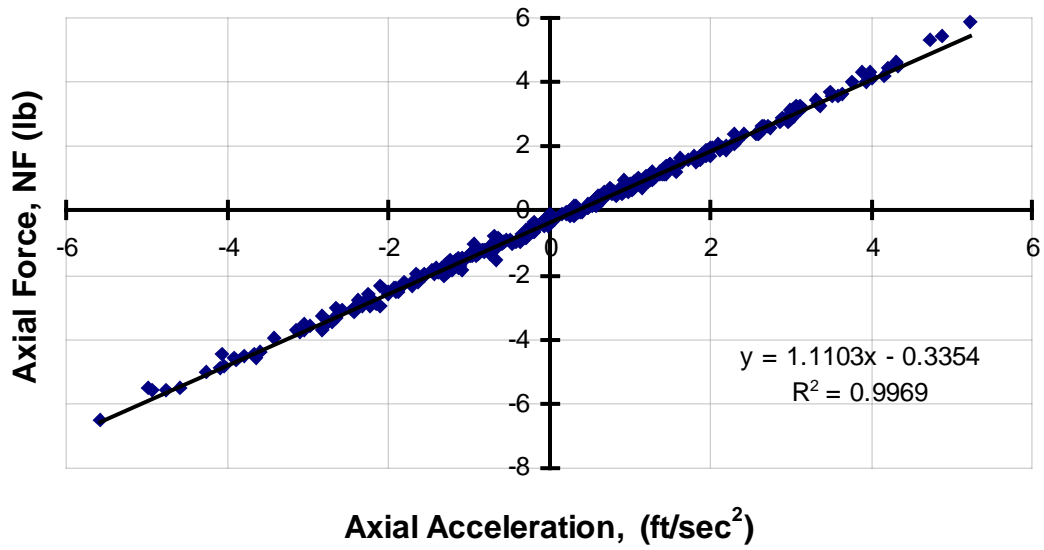


Figure A7. Pitch Calibration, Normal Force, secondary correction applied.

### Axial Acceleration

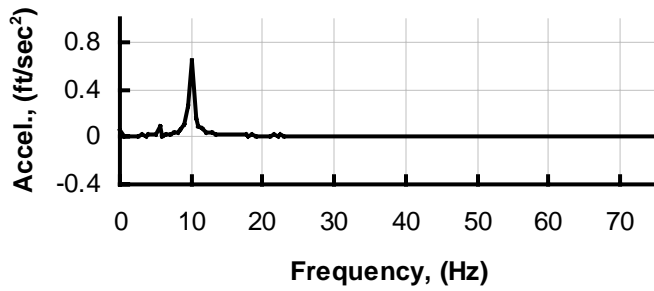


Figure A8. TCA wing spectral analysis of axial acceleration.

### Axial Force

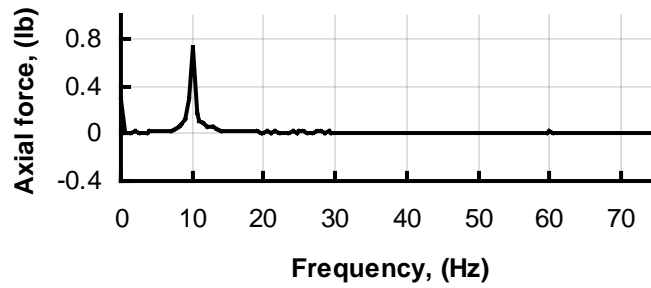


Figure A9. TCA wing spectral analysis of axial force, no correction.

### Corrected Axial Force

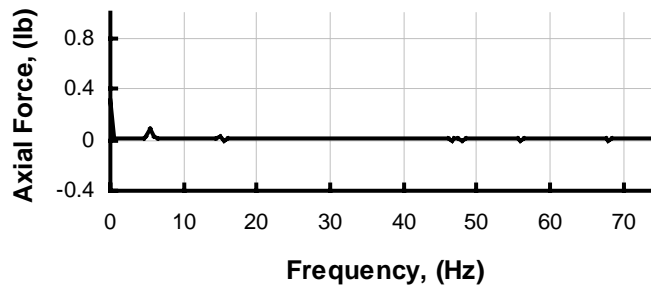


Figure A10. TCA wing spectral analysis of axial force, primary correction.

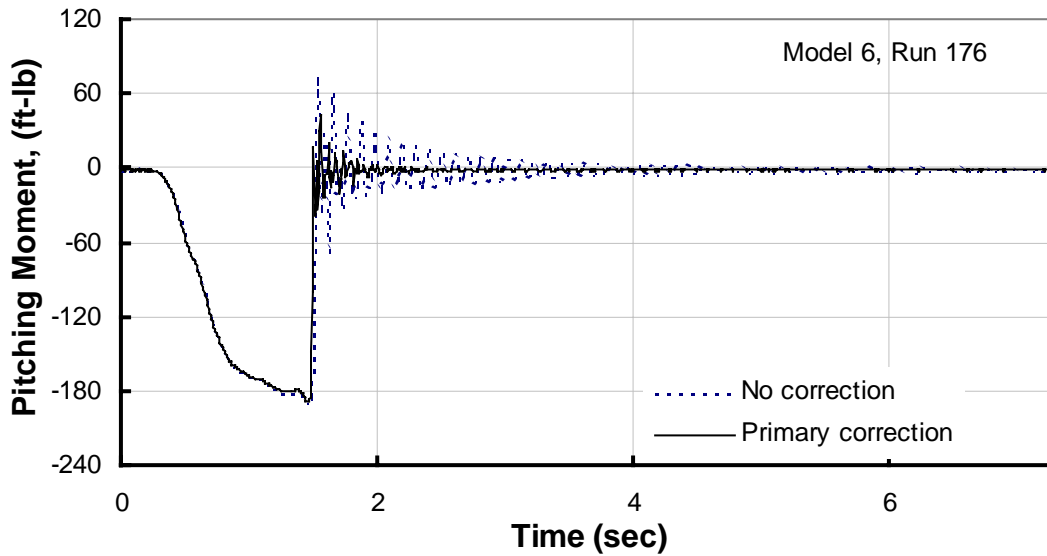


Figure A11. TCA wing inertial loads correction for pitching moment.

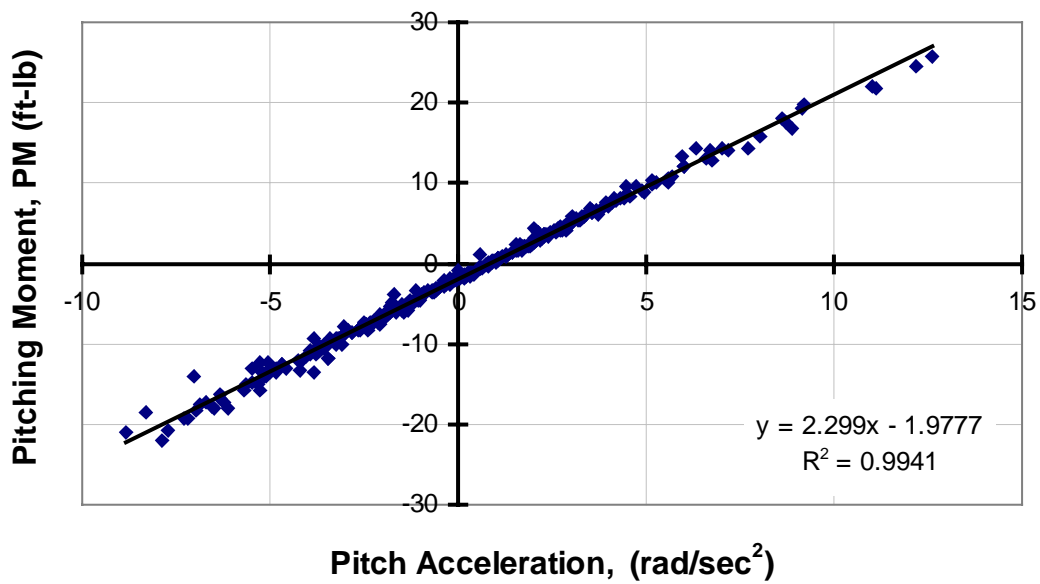


Figure A12. Correlation between pitching moment and pitch acceleration.

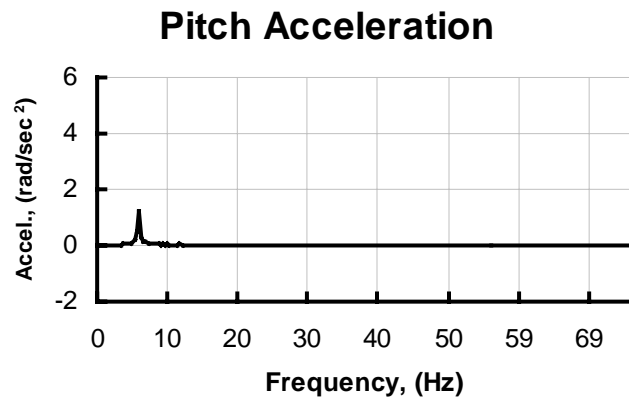


Figure A13. TCA wing spectral analysis of pitch acceleration.

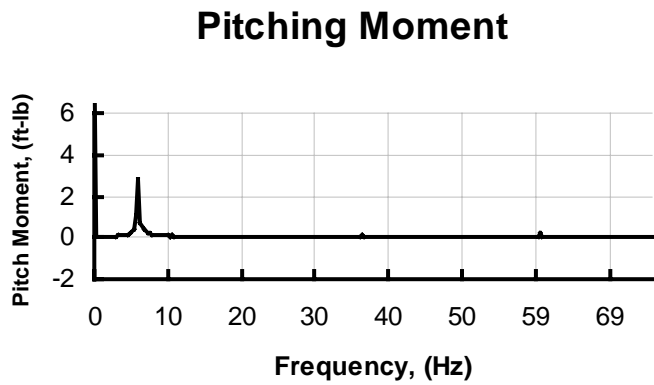


Figure A14. TCA wing spectral analysis of pitching moment, no correction.

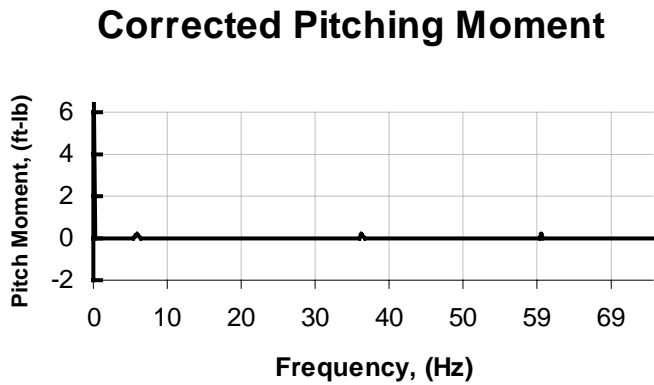


Figure A15. TCA wing spectral analysis of pitching moment, primary correction.

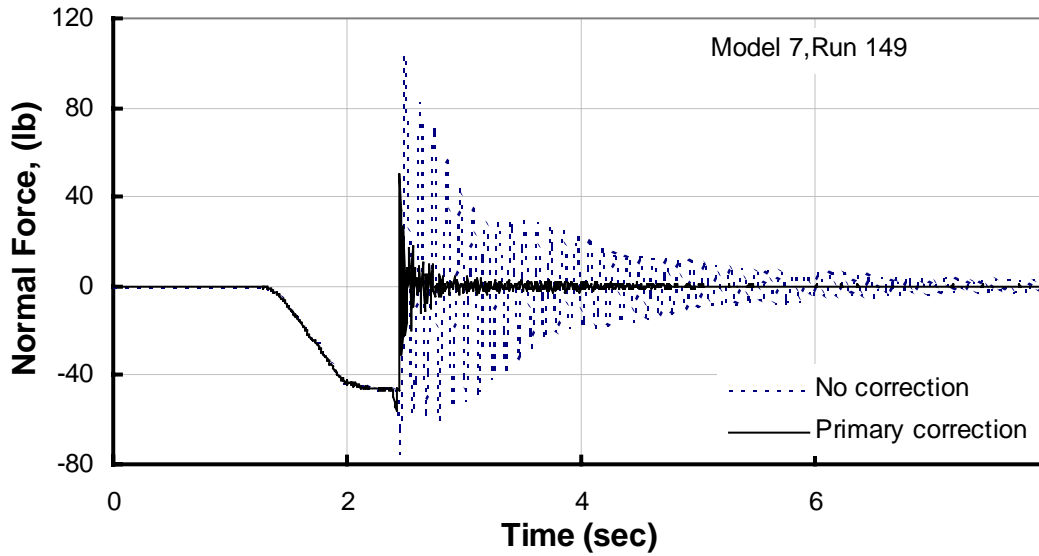


Figure A16. TU-144 wing inertial loads correction for normal force.

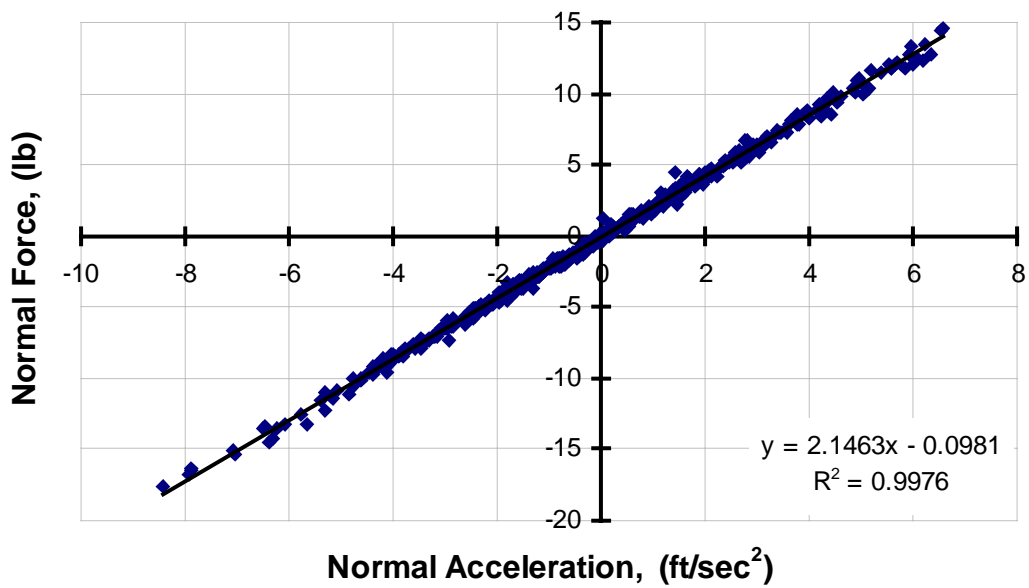


Figure A17. TU-144 wing correlation between normal force and normal acceleration.

## NORMAL ACCELERATION

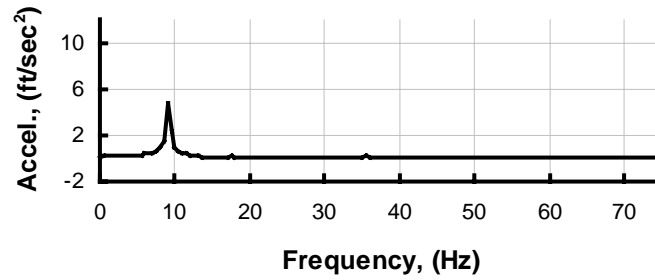


Figure A18. TU-144 wing spectral analysis of normal acceleration.

## NORMAL FORCE

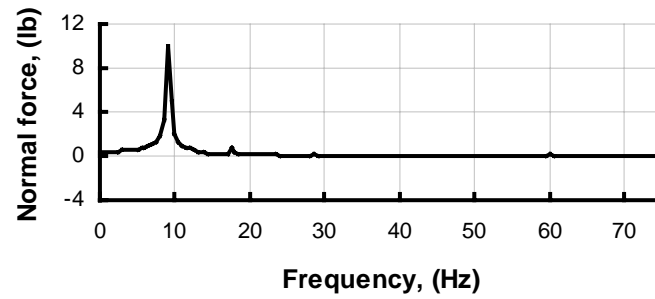


Figure A19. TU-144 wing spectral analysis of normal force, no correction.

## CORRECTED NORMAL FORCE

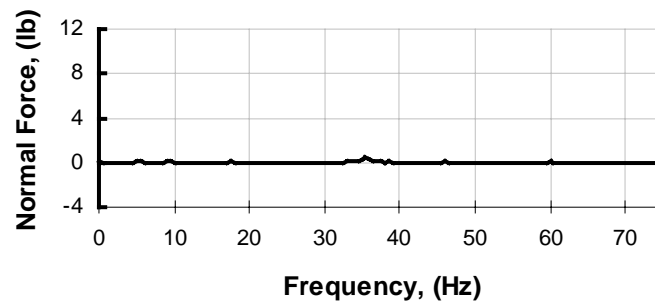


Figure A20. TU-144 wing spectral analysis of normal force, primary correction.

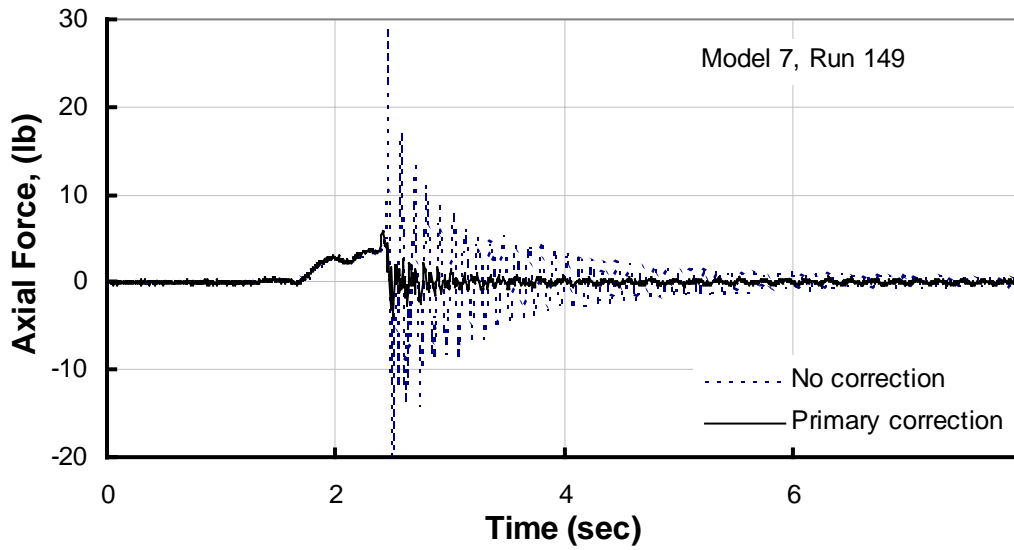


Figure A21. TU-144 wing inertial loads correction for axial force.

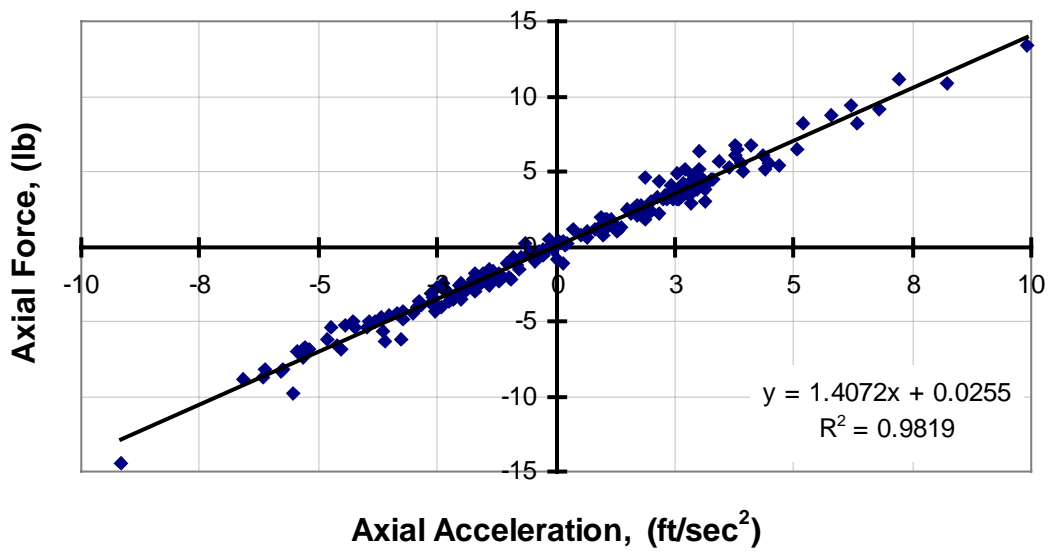


Figure A22. Correlation between axial force and axial acceleration.

## AXIAL ACCELERATION

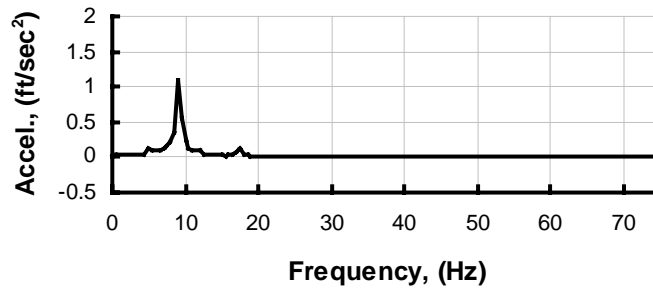


Figure A23. TU-144 wing spectral analysis of axial acceleration.

## AXIAL FORCE

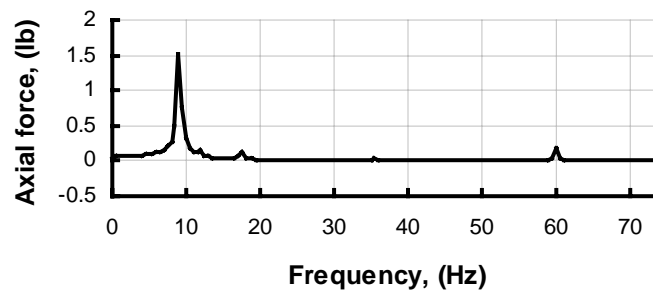


Figure A24. TU-144 wing spectral analysis of axial force, no correction.

## CORRECTED AXIAL FORCE

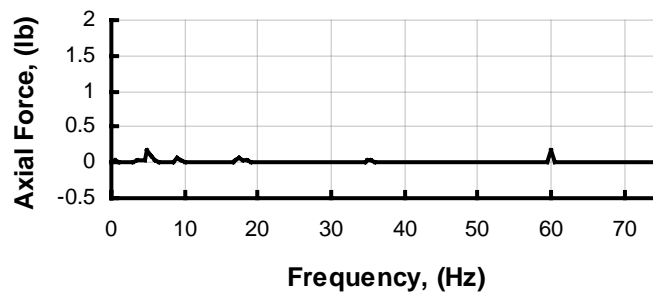


Figure A25. TU-144 wing spectral analysis of axial force, primary correction.

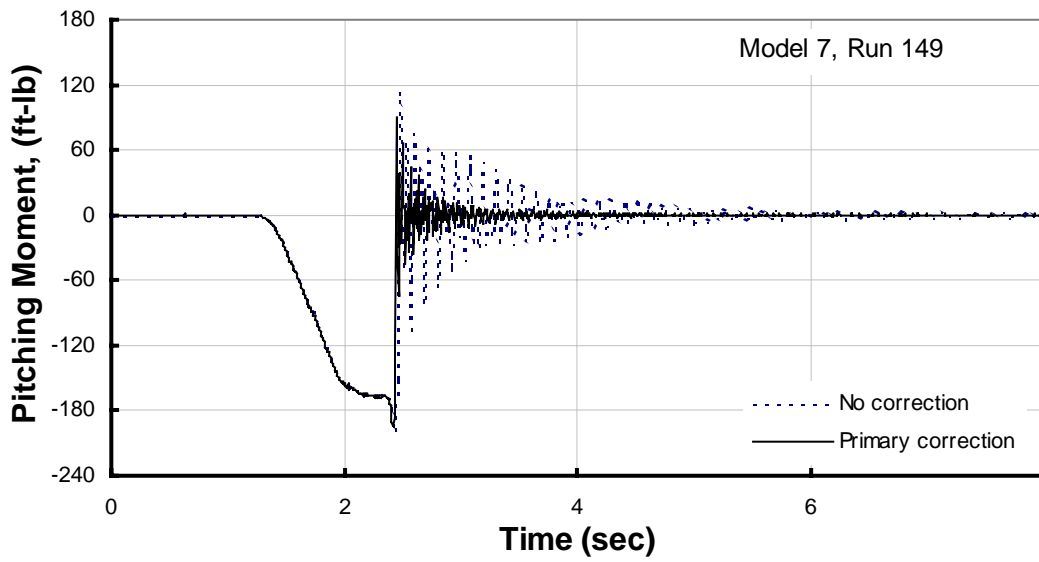


Figure A26. TU-144 wing inertial loads correction for pitching moment.

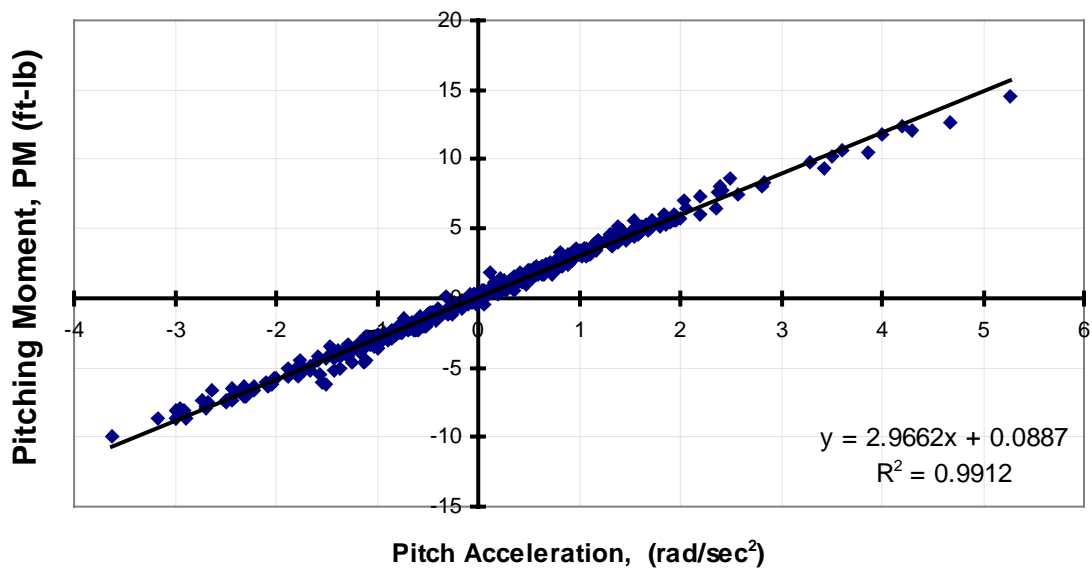


Figure A27. TU-144 wing correlation between pitching moment and pitch acceleration.

### Pitch Acceleration

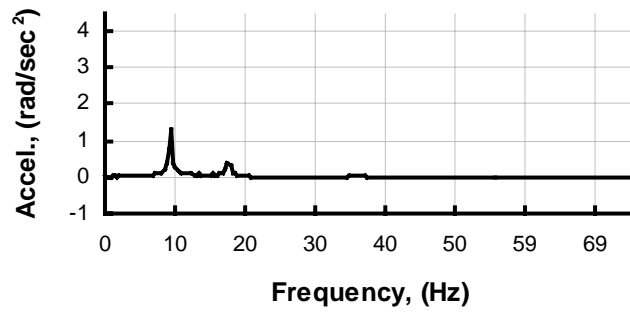


Figure A28 Spectral Analysis of Pitch Acceleration.

### Pitching Moment

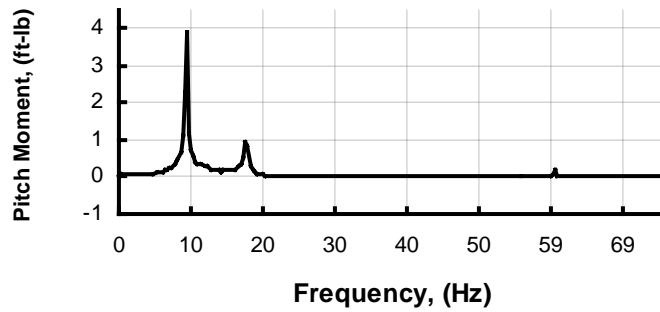


Figure A29 Spectral Analysis of Pitching Moment, no correction.

### Corrected Pitching Moment

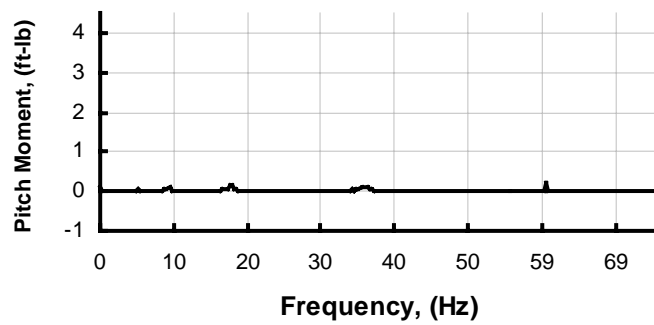


Figure A30 Spectral Analysis of Pitching Moment, primary correction.

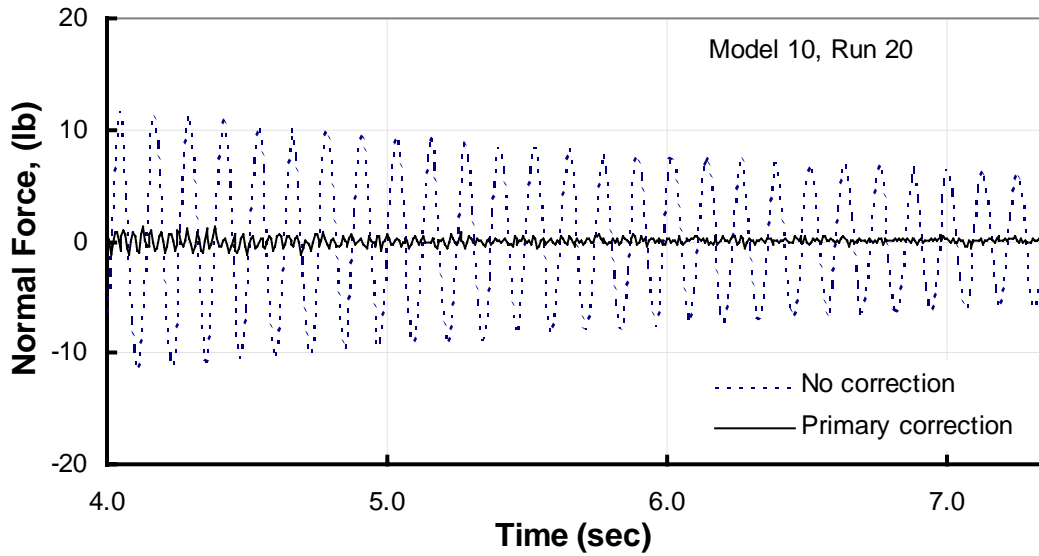


Figure A31. Elliptical wing inertial loads correction for normal force.

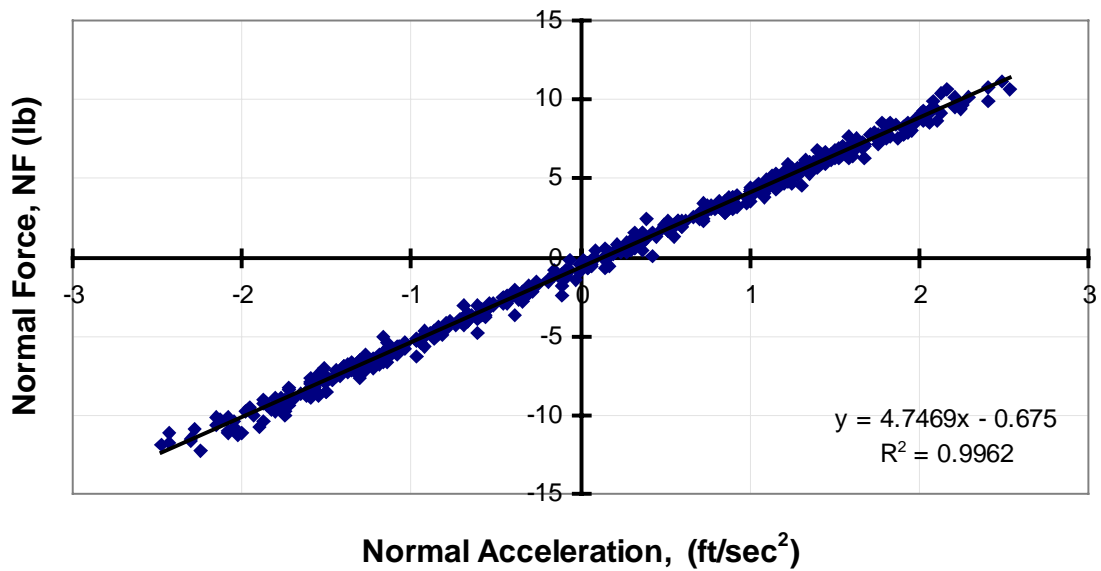


Figure A32. Elliptical wing correlation between normal force and normal acceleration.

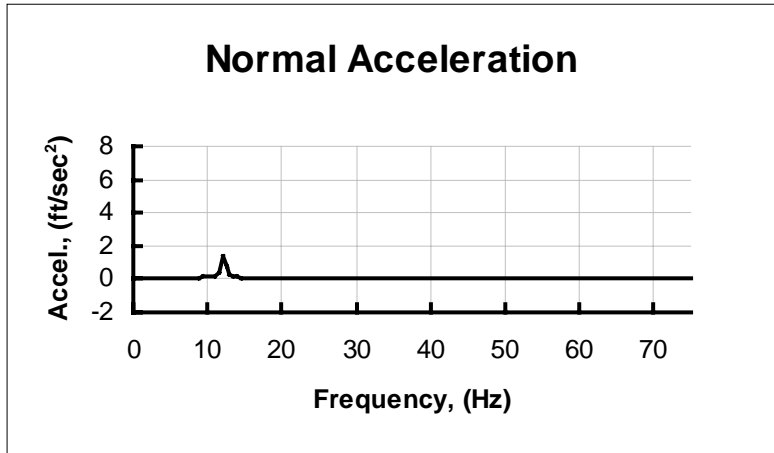


Figure A33. Elliptical wing spectral analysis of normal acceleration.

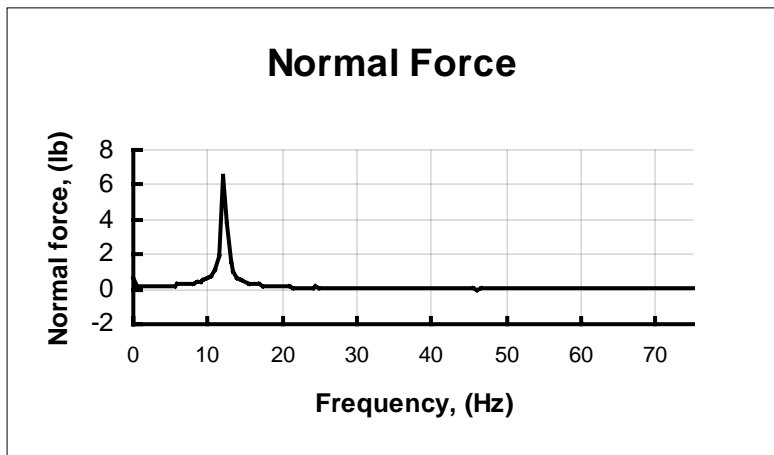


Figure A34. Elliptical wing spectral analysis of normal force, no correction.

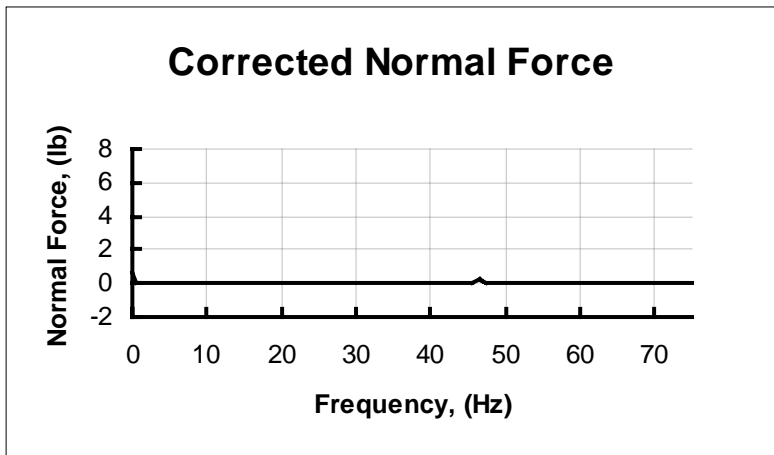


Figure A35. Elliptical wing spectral analysis of normal force, primary correction.

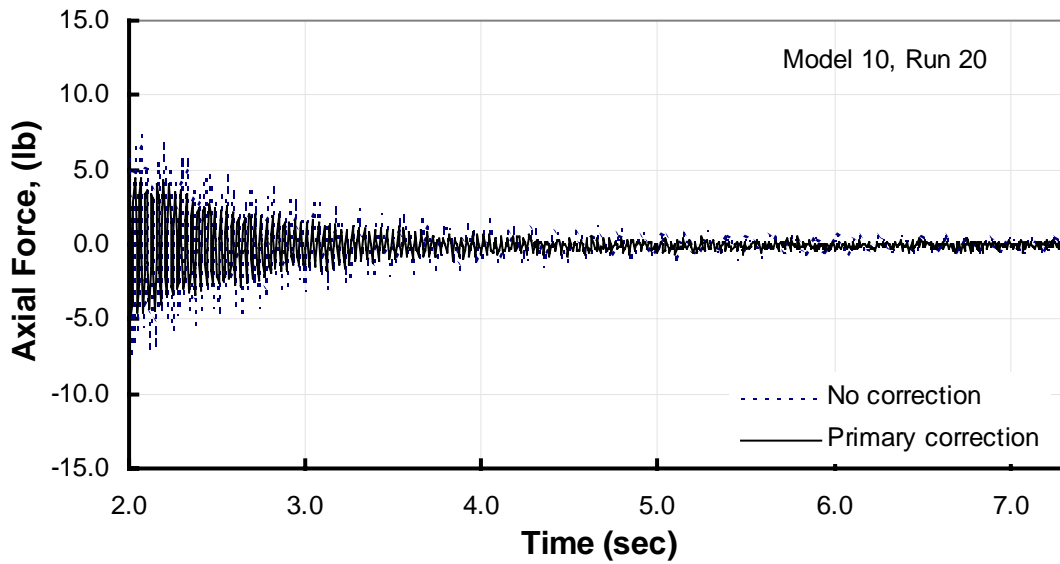


Figure A36. Elliptical wing inertial loads correction for axial force.

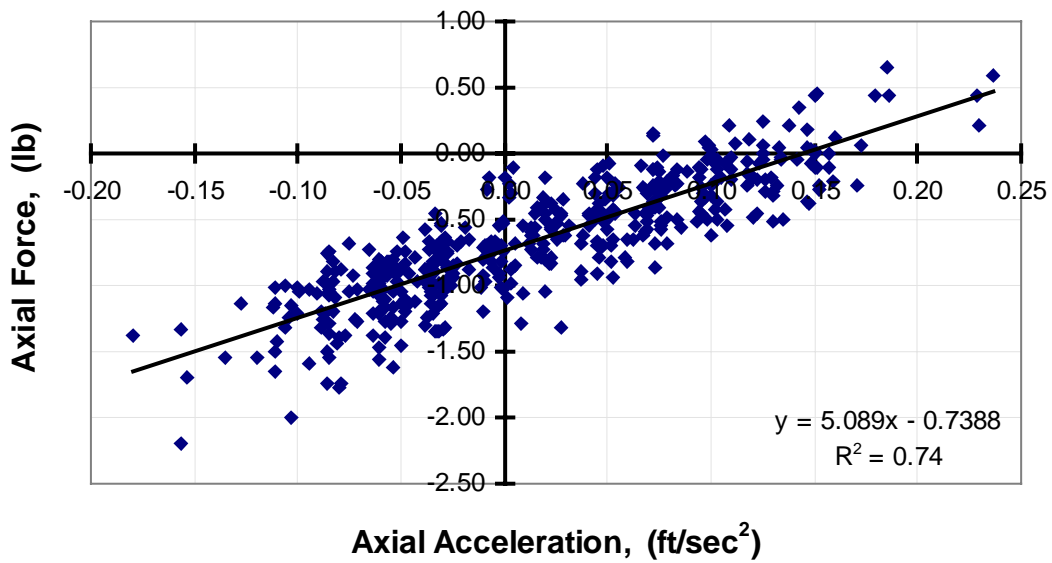


Figure A37. Elliptical wing correlation between axial force and axial acceleration.

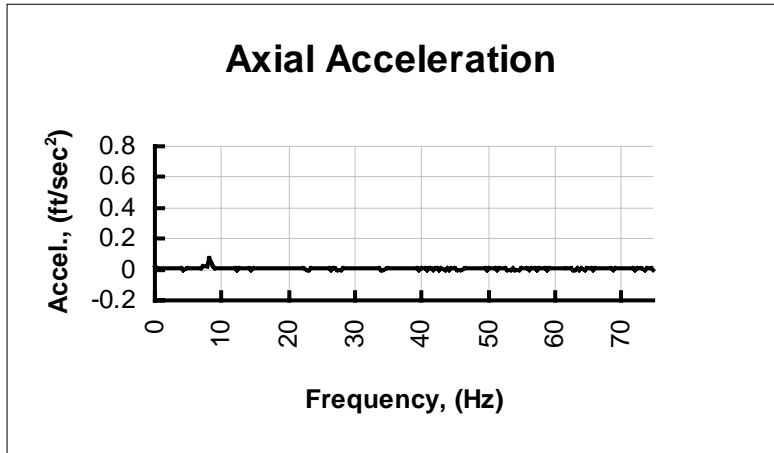


Figure A38. Elliptical wing spectral analysis of axial acceleration.

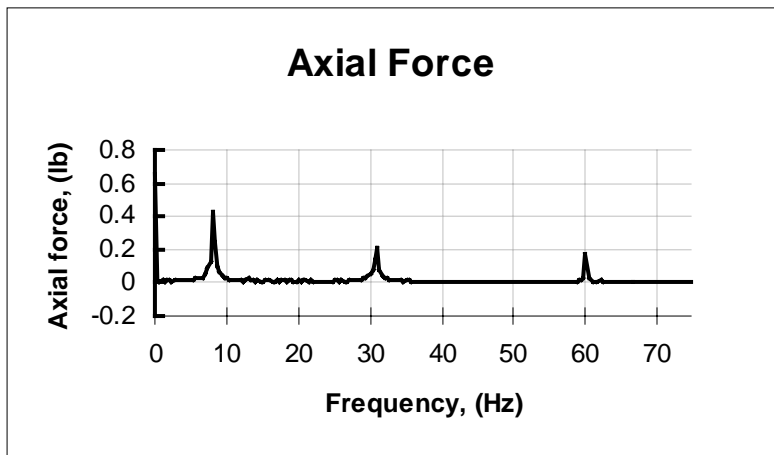


Figure A39. Elliptical wing spectral analysis of axial force, no correction.

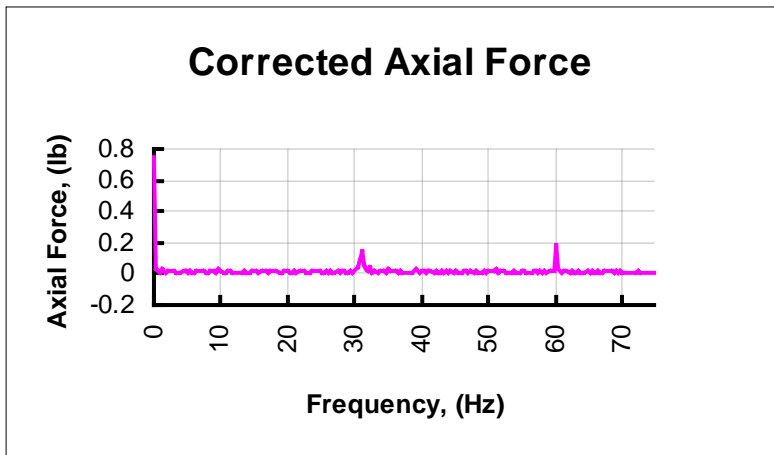


Figure A40. Elliptical wing spectral analysis of axial force, primary correction.

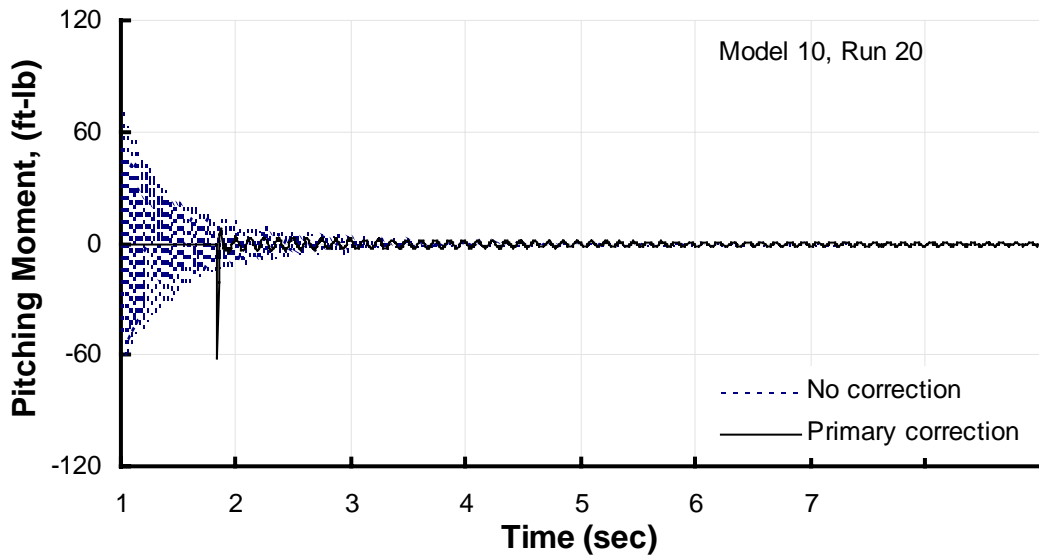


Figure A41. Elliptical wing inertial loads correction for pitching moment.

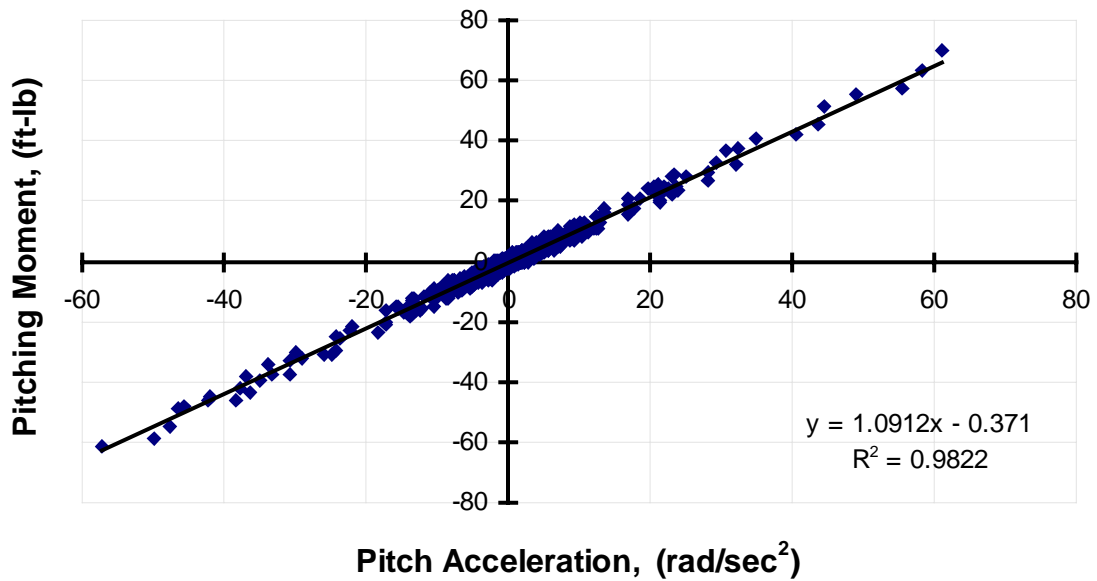


Figure A42. Correlation between pitching moment and pitch acceleration.

### Pitch Acceleration

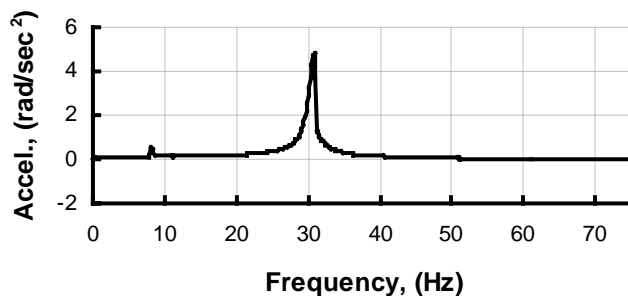


Figure A43. Elliptical wing spectral analysis of pitch acceleration.

### Pitching Moment

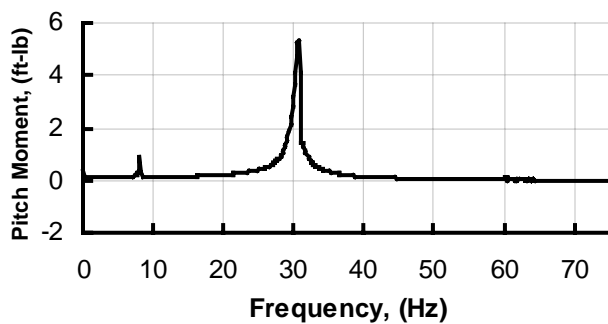


Figure A44. Elliptical wing spectral analysis of pitching moment, no correction.

### Corrected Pitching Moment

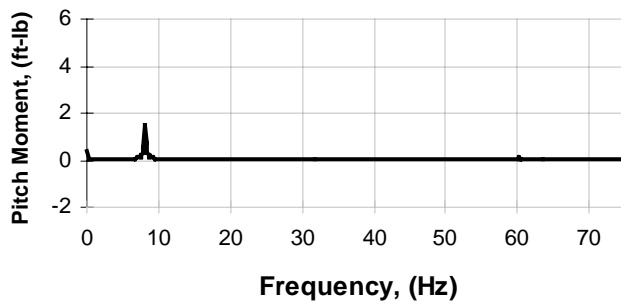


Figure A45. Elliptical wing spectral analysis of pitching moment, primary correction.

## APPENDIX B Post-Processing data using comboa

### B.1 Logon Procedure

Enter user id:           dgetest

Enter password:

### B.2 Setting up the Comboa Processing Directory

*Directory:*                   export/home/dge

*Required input files:*       groups.pre  
                                  groups.1422  
                                  comboa  
                                  inxxx

*Output files:*                answer  
                                  logcomboa  
                                  outcomboa  
                                  euinfo  
                                  windoff.log

### B.3 Defining the inxxx file

```
csfile cs486
rpfile rptname
rawfile TEST46200229
229   -1    -1    2
YES
NO
NO
PR ALL
-1
```

#### B.3.1 rptname file

The rptname file is used to specify the parameters to be processed for each run. A report is

generated for the selected parameters and is called *outcomboa*.

#### **B.4 Comboa user interface**

From cmdtool window:

```
Type   comboa  
Enter Operator Input File Name: inxxx  
      STOP: Normal Termination of COMBOA!
```

## APPENDIX C Post Processing data using dynamic

The software package *dynamic* performs post processing of dynamic data collected from force-balance and accelerometer outputs. The program reads the most current *answer* data file created by *comboa* in the same directory. The following files are required for *dynamic* to function:

accelr.F	acceleration calculations and zero offset cal from run XXX
dynam.F	data reduction parameters such as lift and drag coefficients
dynamic.F	main processing unit
ifind.F	finds parameters in answer
inertia.F	performs a multivariate regression to calc moments of inertia
intgrt.F	integrates accelerations to calculate velocities
ipracc.F	outputs accelerations
iprbal.F	output balance forces
iprsig.F	output signals
iprvel.F	output velocities
linear.F	performs mass calculations
pm.F	called by inertia, perfoms multivariate regression
prload.F	calculates aerodynamic loads
readd.F	reads answer
rjusty.F	right justifies search field
rm.F	3-component multivariate regression
rmld.F	subroutine to filter the inertial loads out of the measurements
setupd.F	reads model configuration file
config6.inp	model 6 configuration file
config7.inp	model 7 configuration file
config10.inp	model 8 configuration file

groups.i  
params.i  
symfup.i

### ***Input File***

answer

### ***Output File naming convention***

runXXX_YYY_acc	-Accelerometer data from run Y
runXXX_YYY_dyn	-Processed lift, drag coefficients, alpha, sink rate
runXXX_YYY_lng	-Longitudinal (Normal, Axial, and Pitch) loads and accelerations
runXXX_YYY_ltd	-Lateral (Roll, Yaw, and Side) loads and accelerations measured

runXXX_YYY_ld	-Velocities
runXXX_YYY_vel	-Balance data in voltage form as it was acquired
runXXX_YYY_g	-Accelerometer signals

The subroutine first goes through a linear regression scheme of the three force equations to calculate the mass of the model. In these equations, m is the mass of everything on the model side of the strain gauge of the balance. The program then uses Multivariate regression to solve for the inertias and centroid positions involved in the three moment equations. The scheme used for solving for these constants was to solve for the most significant terms. Therefore, I<sub>y</sub> (y-Inertia) in the pitching moment equation was calculated first, then I<sub>x</sub> (x-Inertia) in the rolling moment equation and finally I<sub>z</sub> (z-Inertia) in the yawing moment equation. The centroid positions were being calculated along with each of the inertias. The multivariate regression scheme has the following form:

$$y = b_1 * x_1 + b_2 * x_2 + b_3 * x_3$$

where,      b<sub>1</sub>, b<sub>2</sub>, b<sub>3</sub> -regression constants (Inertias, centroid positions)

            x<sub>1</sub>, x<sub>2</sub>, x<sub>3</sub> -independent variables (acceleration data arrays)

            y            -dependent variable (moment data arrays)

Once the constants are calculated, they are used to subtract the inertial loads from the total loads in file runY.ld. The resulting residual loads are then formatted into a file which PREPLOT can easily read. The file is composed of two zones. The first zone is the total loads and the second is the residual loads.

Since the mass of the model, inertias and centroid positions are calculated with subroutine inertia, cards 5 and 6 in the configuration file (configY.inp) are not necessary. However, the distances, dist(i), from the accelerometers to the model's center of gravity will still need to be measured since they are used in the subroutine ACCELR.

## C.1 Setting up the Dynamic Processing Directory

Several model dependent configuration files are required in order to properly perform calculations:

Model 6:	config6.inp
Model 7:	config7.inp
Model 10:	config10.inp

### ***Model configuration file***

The model configuration file (configxx.inp) contains the following information:

x distance from balance moment reference center to six accelerometers (in inches)

y distance from balance moment reference center to six accelerometers (in inches)

z distance from balance moment reference center to six accelerometers (in inches)

accelerometer sensitivities (these were configured as -1.0 if the accelerometer was placed upside down)

mass (slugs) as calculated by the calibration runs for each model

Moments of inertia as calculated by the calibration runs for each model. (slug-ft<sup>2</sup>)

Wing Area (ft<sup>2</sup>) SAREA1, BSPAN1 (inches) and Reference chord length, CHORD1 (inches)

### ***Model 6 configuration file***

card 1 - x distance from balance to accel

2.264 2.264 3.264 14.736 15.736 16.436

card 2 y distance from balance to accel

5.5 0 0 0 0

card 3 z distance from balance to accel

-2.638 -2.638 -2.375 -2.638 -2.375 -2.375

card 4 x,y,z distance from balance to cg

0 0 -2.5

card 5 accel sensitivities

1.0 1.0 -1.0 1.0 1.0 1.0 1.0 1.0 1.0

card 6 mass (slugs)

1.132 1.759 1.8531

card 7 Ixx Iyy Izz Ixz slug-ft<sup>2</sup> reference to mrc

0.6299 2.3319 2.6956 -0.001

card 8      Sarea   bspan   chord  
 7.894      48.0   34.723

***Model 7 configuration file***

Card 1 - x distance from balance to accel  
 -2.00      -2.00   -3.00   15.00   16.00   16.25

card 2      y distance from balance to accel  
 5.5 0      0      0      0      0

card 3      z distance from balance to accel  
 -2.638      -2.638   -2.375   -2.638   -2.375   -2.375

card 4      x,y,z distance from balance to cg  
 0   0      0

card 5      accel sensitivities  
 1.0 1.0   -1.0   1.0   1.0   1.0   1.0   1.0   1.0   1.0

card 6      mass (slugs)  
 1.347      1.987   2.144

card 7      Ixx Iyy Izz      Ixz      slug-ft2 reference to mrc  
 1.133      2.968   3.658   -0.025

card 8      Sarea   bspan   chord  
 9.466      47.1   38.25

***Model 10 configuration file***

card 1 - x distance from balance to accel  
 0   0      29.03   11.65   11.65   16.53

card 2      y distance from balance to accel  
 2.625      0      1.75   0      1.75   0

card 3	z distance from balance to accel (not applicable)									
-2.638	-2.638	-2.375	-2.638	-2.375	-2.375					
card 4	x,y,z distance from balance to cg									
0	0	0								
card 5	accel sensitivities									
1.0	1.0	-1.0	1.0	1.0	1.0	1.0	1.0	1.0	1.0	1.0
card 6	mass (slugs)									
1.347	1.987	2.144								
card 7	Ixx	Iyy	Izz	Ixz	slug-ft2 reference to mrc					
1.133	2.968	3.658	-0.025							
card 8	Sarea	bspan	chord							
6.448	80.622	12.331								

## APPENDIX D Accelerometers

Accelerometer sensitivity coefficients

AccelerometerSerial Number	Sensitivity coefficients (V/g)
10861	0.1999
10862	0.1998
10863	0.2005
10864	0.2014
10865	0.1987
10866	0.2003
10867	0.1995
10868	0.1997
11671	0.19805
11672	0.19933
11673	0.19932
11674	0.20171
11675	0.20012
11676	0.19939
11677	0.19827
11678	0.19918

<b>VARIABLE ACCELEROMETER</b>	<b>CAPACITANCE</b>	<b>Specification</b>
<b>Model</b>		7290A-10
<b>Range</b>		±10g
<b>Frequency Response</b>		0-500
<b>Full Scale Output</b>		±2V
<b>Non-linearity and Hysteresis</b>		±0.20

Accelerometer Orientation

<b>Model-*</b>	<b>Position</b>	<b>Toward Right Wing</b>	<b>Down</b>	<b>Forward</b>
<b>6,7</b>	Model	3,5	1,2,4	6
	Balance	9	7,8	10
<b>10</b>	Model	3,5	2,4	6
	Balance	9	7,8	10

---

## References

- 1 Roskam, J., Airplane Design Part VIII: Airplane Cost Estimation: Design, Development, Manufacturing and Operating. RAEC, Ottawa, Kansas, 1990.
- 2 Pope, Alan, Rae, William H., Jr., Low-Speed Wind Tunnel Testing. Wiley-Interscience, USA, 1984.
- 3 Kemp, W. B., Lockwood, V.E., and Phillips, W. P. "Ground Effects Related to Landing of Airplanes with Low-Aspect Ratio Wings," NASA TN D-3583, October 1966.
- 4 Chang, Ray Chung, An Experimental Investigation of Dynamic Ground Effect. University of Kansas, 1985, pp. 26.
- 5 Gentry, Garl L., Jr., Quinto, P. Frank, Gatlin, Gregory M., and Applin, Zachary T., The Langley 14- by 22- Foot Subsonic Tunnel: Description, Flow Characteristics, and Guide for Users, NASA Technical Paper 3008, September, 1990.
- 6 Gainer, Thomas G., Hoffman, Sherwood, Summary of Transformation Equations and Equations of Motion Used in Free-Flight and Wind-Tunnel Data Reduction and Analysis. NASA SP-3070, 1972, p.25.
- 7 Gainer, Thomas G., Hoffman, Sherwood, Summary of Transformation Equations and Equations of Motion Used in Free Flight and Wind Tunnel Data Reduction and Analysis. NASA SP-3070, 1972, p. 57.
- 8 Hamming, R.W., Digital Filters, Prentice-Hall, Inc., Englewood Cliffs, New Jersey, 1983.
- 9 Baker, Paul A., Schweikhard, William G., and Young, William R., Flight Evaluation of Ground Effect on Several Low-Aspect Ratio Airplanes, NASA TN-D-6053, Oct 1970.
- 10 Lee, Pai-Hung, Lan, C. Edward, and Muirhead, Vincent U., An Experimental Investigation of Dynamic Ground Effect, NASA CR-4105, 1987.
- 11 Chang, Ray Chung and Muirhead, Vincent U., Effect of Sink Rate on Ground Effect of Low-Aspect Ratio Wings, J. of Aircraft, vol. 24, no. 3, Mar 1986, pp. 176-180.
- 12 Kemmerly, Guy T. and Paulson, J. W., Jr., Investigation of Moving-Model Technique for Measuring Ground Effects, NASA TM-4080, 1989.
- 13 Curry, Robert E., Moulton, Bryan J., and Kresse, John, An In-Flight Investigation of Ground Effect on a Forward-Swept Wing Airplane, NASA TM-101708, Sept. 1989.
- 14 Corda, Stephen, Stephenson, Mark T., Burcham, Frank W., and Curry, Robert E., Dynamic Ground Effects Flight Test of an F-15 Aircraft, NASA TM-4604, Sept. 1994.
- 15 van Dam, C.P., Vijgen, P.M.H.W., and Holmes, B.J., Wind Tunnel Investigation on the Effect of the Crescent Planform Shape on Drag, AIAA-90-0300, p. 12
- 16 Kemmerly, Guy T., Dynamic Ground Effect Measurements on the F-15 STOL and Maneuver Technology Demonstrator (S/MTD) Configuration. NASA TP 3000, 1987.

REPORT DOCUMENTATION PAGE			Form Approved OMB No. 0704-0188	
Public reporting burden for this collection of information is estimated to average 1 hour per response, including the time for reviewing instructions, searching existing data sources, gathering and maintaining the data needed, and completing and reviewing the collection of information. Send comments regarding this burden estimate or any other aspect of this collection of information, including suggestions for reducing this burden, to Washington Headquarters Services, Directorate for Information Operations and Reports, 1215 Jefferson Davis Highway, Suite 1204, Arlington, VA 22202-4302, and to the Office of Management and Budget, Paperwork Reduction Project (0704-0188), Washington, DC 20503.				
1. AGENCY USE ONLY (Leave blank)		2. REPORT DATE August 1999	3. REPORT TYPE AND DATES COVERED Contractor Report	
4. TITLE AND SUBTITLE Investigation of a Technique for Measuring Dynamic Ground Effect in a Subsonic Wind Tunnel			5. FUNDING NUMBERS NCC1-24  537-07-51-02	
6. AUTHOR(S) Sharon S. Graves				
7. PERFORMING ORGANIZATION NAME(S) AND ADDRESS(ES) The George Washington University Joint Institute for Advancement of Flight Sciences Langley Research Center, Hampton, Virginia 23681-2199			8. PERFORMING ORGANIZATION REPORT NUMBER	
9. SPONSORING/MONITORING AGENCY NAME(S) AND ADDRESS(ES)  National Aeronautics and Space Administration NASA Langley Research Center Hampton, VA 23681-2199			10. SPONSORING/MONITORING AGENCY REPORT NUMBER  NASA/CR-1999-209544	
11. SUPPLEMENTARY NOTES Graves: Graduate Research Scholar Assistant, GW JIAFS. This research was conducted in partial satisfaction of the requirements for the degree of Master of Science with The George Washington University. Langley Technical Monitor: Edgar G. Waggoner				
12a. DISTRIBUTION/AVAILABILITY STATEMENT Unclassified-Unlimited Subject Category 02                      Distribution: Nonstandard Availability: NASA CASI (301) 621-0390			12b. DISTRIBUTION CODE	
13. ABSTRACT (Maximum 200 words) To better understand the ground effect encountered by slender wing supersonic transport aircraft, a test was conducted at NASA Langley Research Center's 14 x 22 foot Subsonic Wind Tunnel in October, 1997. Emphasis was placed on improving the accuracy of the ground effect data by using a "dynamic" technique in which the model's vertical motion was varied automatically during wind-on testing. This report describes and evaluates different aspects of the dynamic method utilized for obtaining ground effect data in this test. The method for acquiring and processing time data from a dynamic ground effect wind tunnel test is outlined with details of the overall data acquisition system and software used for the data analysis. The removal of inertial loads due to sting motion and the support dynamics in the balance force and moment data measurements of the aerodynamic forces on the model is described. An evaluation of the results identifies problem areas providing recommendations for future experiments. Test results are validated by comparing test data for an elliptical wing planform with an Elliptical wing planform section with a NACA 0012 airfoil to results found in current literature. Major aerodynamic forces acting on the model in terms of lift curves for determining ground effect are presented. Comparisons of flight and wind tunnel data for the TU-144 are presented.				
14. SUBJECT TERMS Dynamic Ground Effect; Subsonic Wind Tunnel Test; Data Acquisition System			15. NUMBER OF PAGES 66	
			16. PRICE CODE A04	
17. SECURITY CLASSIFICATION OF REPORT Unclassified	18. SECURITY CLASSIFICATION OF THIS PAGE Unclassified	19. SECURITY CLASSIFICATION OF ABSTRACT Unclassified	20. LIMITATION OF ABSTRACT	